Advanced Materials

ADVANCED MATERIALS
www.advmat.de

PERSPECTIVE OPEN ACCESS

Energetic Offset in Organic Solar Cells- Importance, Confusion and Outlook

Nakul Jain[1] | Xian'e Li[2] | Mats Fahlman[2] | Olle Inganäs[1] | Koen Vandewal[3] | Feng Gao[1]

[1]Department of Physics, Chemistry and Biology (IFM), Linköping University, Linköping, Sweden | [2]Laboratory of Organic Electronics, Department of Science and Technology (ITN), Linköping University, Norrköping, Sweden | [3]Institute for Materials Research (imo-imomec), Hasselt University, Diepenbeek, Belgium

Correspondence: Nakul Jain (nakul.jain@liu.se) | Feng Gao (feng.gao@liu.se)

Received: 1 September 2025 | **Revised:** 5 May 2026 | **Accepted:** 6 May 2026

Keywords: charge generation | energetic offset | non-radiative loss | organic solar cells | voltage loss

ABSTRACT

The energetic offset between donor (D) and acceptor (A) is one of the most important parameters which influences the charge generation and voltage loss, and hence overall performance of the organic solar cells (OSCs). However, the different methodologies/techniques used to determine this offset provides a wide range of values, even for the same D:A system. This creates confusion in the community and makes it difficult to make comparisons between different labs. This discrepancy arises because each technique probes fundamentally different physical processes and because of the limited understanding of interfacial energy level alignment, particularly at buried interfaces. In this perspective, we discuss the pros and cons of the frequently used methods/techniques that are used to determine the offset, and their underlying principles. We identify temperature-dependent electro-optical techniques as a reasonable method which can help to achieve a consistent comparison between different material systems. In order to minimize the voltage losses of organic photovoltaics below 0.5 V, we suggest that the focus should be on designing low bandgap molecules with inherently high photoluminescence quantum yield and ensuring that the donor:acceptor blends exhibit strong luminescence efficiency.

1 | Introduction

Organic solar cells (OSCs), composed of donor (D) and acceptor (A) excitonic materials, have experienced tremendous progress in the past decade, with power conversion efficiencies now approaching 21% [1–7]. This has been made possible largely by the development of non-fullerene acceptors (NFAs) [8, 9]. Compared with conventional fullerene-based acceptors, NFA-based OSCs show enhanced short-circuit current densities (J_{SC}) and decreased voltage losses (hence improved open-circuit voltages V_{OC}), resulting in efficiencies nearly twice as high as those of the best fullerene-based OSCs [4, 7, 10, 11]. From the materials point of view, a parameter which is closely related with both J_{SC} and V_{OC} enhancement in NFA-based OSCs is the energetic offset between D and A materials- a parameter which unfortunately causes a lot of confusion.

The energetic offset plays a central role in charge separation and recombination dynamics [12–15]. In the best performing OSCs, donor:NFA blends with small energetic offsets exhibit efficient exciton dissociation (and thus effective photocurrent generation) as well as decreased voltage losses [8, 9]. Traditionally, for fullerene-based OSCs, an empirical limit of offset of more than 0.3 eV has been determined, below which charge separation

---

This work is dedicated to Professor Paul Blom on the occasion of his 60th birthday. We greatly appreciate his pioneering contributions to organic electronic devices. F.G. has been particularly inspired by Professor Blom's ability to communicate device physics with clarity, offering compelling physical insights and intuitive pictures.

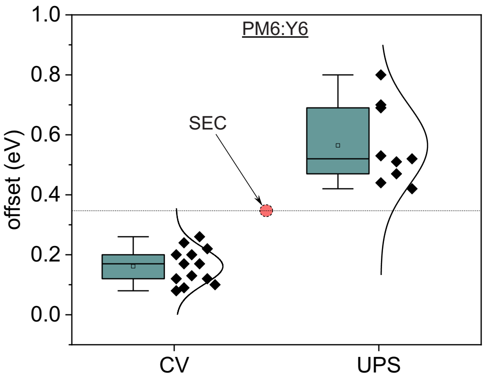

FIGURE 1 | HOMO Offset measured by cyclic voltammetry (CV), and ultraviolet photoelectron spectroscopy (UPS) method for neat PM6 and Y6 films by the different groups (Table S1). The red circle shows the offset value measured by the spectroelectrochemical (SEC) method for neat PM6 and Y6 film.

becomes inefficient [16–20]. The need for such a high energetic offset leads to a decreased effective gap (determined by the energy of charge-transfer states) and severe non-radiative recombination loss (because of strong wavefunction overlap between the charge-transfer state and ground state) in optimized fullerene based devices, leading to large voltage losses (>0.7 V) [21–23]. In contrast, NFA-based OSCs and novel donors like P(DPP6DOT2-T) [24], PIPCP [25] and PIDTT-TID [26] with fullerene-based OSCs have been demonstrated to work effectively with reduced energetic offset (below the 0.3 eV limit), and even for negligible offsets close to zero as claimed by some reports [27–40]. This leads to an enhanced effective gap in optimized devices and also decreased non-radiative recombination losses, both contributing to lower voltage losses (~ 0.5 eV in some of the best devices [2, 41]). In addition, the realization of efficient charge separation, despite minimal energetic offsets, has stimulated extensive debate regarding the fundamental charge carrier generation mechanisms in these OSCs [42–55].

In spite of the importance of energetic offset for enhanced open-circuit voltage and charge generation, precise determination of energetic offset values has been ambiguous and subject to intense debate [56, 57]. Energetic offsets are typically estimated either from the difference in frontier molecular orbital (FMO) energies (e.g., HOMO-HOMO or LUMO-LUMO offsets between the donor and acceptor, where HOMO; highest occupied molecular orbital and LUMO; lowest unoccupied molecular orbital) or from the energy difference between the local exciton (LE) and the charge-transfer (CT) states. However, these two approaches do not yield equivalent physical interpretations and should not be compared. Further, each method or instrument to calculate the offset has its own pros and cons, including associated errors, which complicate the evaluation of the offset. As a result, different groups are reporting different values of the offset between the donor and acceptor for the same D:A system. As an example for a state-of-the-art PM6:Y6 system, the offset value in literature varies from 0.08 eV to 0.8 eV, a difference of nearly 0.7 eV (Figure 1) [56–75], This creates significant confusion and makes it difficult to compare these values between different material systems. Therefore, gaining a clearer understanding of the underlying causes of these discrepancies and identifying more reliable approaches for determining the energy level offset is the need of the hour.

In this perspective, we discuss different types of energetic offsets, and the techniques commonly used to measure them. We highlight the limitations and potential sources of error, focusing on discrepancies that arise from the different physical quantities probed, the underlying measurement principles, and the interpretation of interfacial energetics. Our analysis suggests that temperature-dependent electro-optical measurements—such as open circuit voltage (V_{OC}-T) and electroluminescence quantum yield (ELQY-T) measurements for calculating the LE-CT offset —offer more consistent and reliable values compared to commonly used techniques, such as electrochemical measurements and ultraviolet photoelectron spectroscopy. We also highlight that the voltage loss of 0.5 eV in state-of-the-art OSCs is not limited by the offset but is rather limited by the low photoluminescence quantum yield (PLQY) of the material. Hence, a novel material design strategy to achieve the high PLQY material is the key for the next-generation OSCs.

2 | Definitions of the Offset

There are two primary methods for representing the energetics of organic donor-acceptor blends—via a FMO energy diagram or a Jablonski energy diagram (Figure 2). The former represents the single-particle energy levels, while the latter illustrates the quasi-particle energy levels [76].

2.1 | The frontier molecular orbital energy diagram

The frontier molecular orbital energy diagram is a representation of the frontier electronic energy levels of a molecule, being the HOMO and LUMO level. The HOMO represents the highest energy level occupied by an electron in a molecule. The energy required to remove an electron from this level—bringing it to the vacuum—is referred to as the ionization energy (IE). While the HOMO level is often used as an approximation for IE, they are not strictly equivalent [77]. When an electron is removed from a molecule, electronic and geometric relaxation (both molecule and lattice relaxation) occurs. Hence, the IE of a molecule is smaller than the HOMO energy of its neutral state. Similarly, the LUMO denotes the lowest energy level available to accept an electron. The energy gained by adding an electron to this level is referred to as the electron affinity (EA). Like the HOMO-IE relationship, the LUMO and EA are conceptually related but not identical [78]. The difference between the HOMO and LUMO represents the electronic bandgap or transport gap of the material. Here, it is worth noting that organic materials have high excitonic binding energy (B_E) and hence the optical bandgap (Eg) is always smaller than the electronic bandgap [77].

In addition, when individual donor and acceptor materials are combined to form a bulk heterojunction, energetic offsets naturally arise due to the differences in their energy levels (Figure 2). These energy differences (offsets)—particularly in the HOMO and LUMO levels—govern charge separation and recombination dynamics at the interface. Further, although offsets exist between

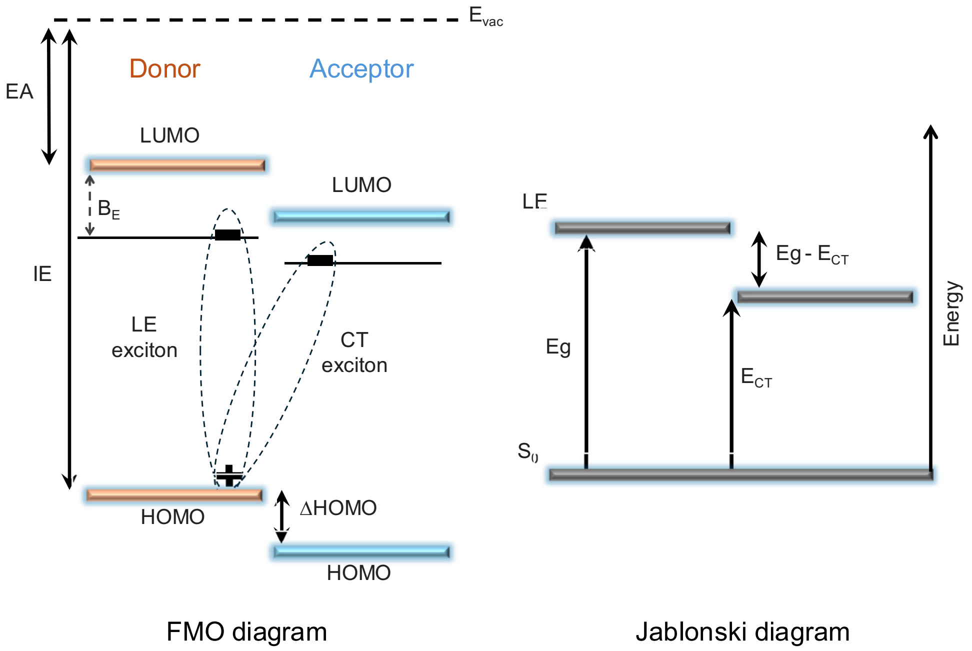

FIGURE 2 | Schematic representation of energy levels in a donor:acceptor system in organic solar cells, illustrated using both the frontier molecular orbital (FMO) level diagram and the Jablonski diagram. (EA; electron affinity, IE; ionization potential, LE; local exciton, CT; charge-transfer, B_E; binding energy, Eg; optical bandgap, E_{CT}; charge-transfer state energy, S0, ground state).

both the HOMO levels (HOMO-offset) and the LUMO levels (LUMO-offset), the primary 'offset of interest' is dictated by the low bandgap component in the D:A blend. This is due to the ultrafast energy transfer from the wide bandgap material to the low bandgap material [57]. Hence the LUMO-offset is the offset of interest in the case of a low-gap donor, and the HOMO-offset becomes the offset of interest in the case of a low-gap acceptor.

2.2 | Jablonski Diagram

Jablonski Diagram is a graphical representation of the excited state energies energy levels of a molecule relative to its electronic and vibronic ground states. Upon photoexcitation, this diagram allows for the visualization of the possible transitions between the states [79, 80]. Hence, it provides a clear understanding of key photophysical processes, including absorption, fluorescence, phosphorescence, vibrational relaxation, charge-transfer and intersystem crossing.

To understand the energetic offset between the donor and acceptor using this method, a simplified Jablonski diagram is presented in Figure 2. Here, the vertical axis represents the energy increasing from the bottom that is, ground state (S_0) to the relevant excited states that is, LE state and CT state. Other states, such as local triplet states and the vibrational levels associated with each electronic state, are omitted from this simplified Jablonski diagram. The LE state (also known as the singlet excitonic state, S1) represents the exciton energy, or the optical bandgap (E_g), of the low bandgap material. The CT state represents the lowest energy level created after a charge (either a hole or an electron) is transferred from one molecule (LE state) to another molecule; upon the transfer, the local exciton is converted into a CT exciton. Therefore, the energetic offset, or the driving force, is represented by the difference between the LE state energy and the CT state energy. The formation of CT excitons is influenced by electrostatic interactions at the donor–acceptor interface, which can lead to a realignment of the molecular energy levels [81]. Therefore, the CT state energy more accurately captures the interfacial energetics of the electron–hole pair, offering a physically relevant measure of the offset.

It is important to note that the HOMO-HOMO or LUMO-LUMO offsets between donor and acceptor materials are not equivalent to the LE-CT energy offset. While HOMO or LUMO offsets describe the energy levels of individual donor and acceptor molecules, the CT state is an intermolecular excited state where the electron and hole are spatially separated across different molecules. The energy of this CT state is not simply derived from the direct subtraction of HOMO of the donor to the LUMO of the acceptor; rather, it is significantly influenced by the Coulombic binding energy between the separated charges and the local dielectric environment. In other words, the relationship between electronic level and excitonic level using a solvent-continuum model can be derived as [82]:

$$E_{CT} = q\left(HOMO_D - LUMO_A\right) - \frac{q^2}{4\pi_{0s} r_{DA}} + \frac{q^2}{8\pi_0}\left(\frac{1}{r_D} + \frac{1}{r_A}\right)\left(\frac{1}{_s} - \frac{1}{_{ref}}\right)$$

here, $HOMO_D$ and $LUMO_A$ correspond to the ionization energy and electron affinity of the donor and acceptor, respectively; ϵ_s is the dielectric constant of the surrounding medium, $\in_{ref}$ is the dielectric constant of the solvent, r_{DA} is the donor–acceptor separation distance, r_D and r_A are the effective molecular radii, ϵ_0 is the vacuum permittivity, and q denotes the elementary charge.

The first term describes the energy difference between the electronic levels of isolated molecules at infinite separation, while the second term accounts for Coulombic attraction between the electron and hole across the donor-acceptor interface. The third term represents the dielectric polarization correction, which stabilizes the CT state depending on the dielectric properties of the surrounding medium and reference solvent. After obtaining this charge-transfer state energy from the above equation, the excitonic offset can be described as:

$$\Delta E_{LE-CT} = E_{LE} - E_{CT}$$

where E_{LE} is the optical bandgap of the low bandgap material and can also be written as Eg or E_{S1}.

This charge-transfer state energy or the excitonic offset highly influences the charge generation as well as the open circuit voltage. Within the framework of Marcus–Levich–Jortner (MLJ) theory, this driving force determines the charge-transfer rate constant [83]:

$$k_{CT} = \frac{2\pi}{\hbar} V^2 \frac{1}{\sqrt{4\pi\lambda kT}} \sum_{m=0}^{\infty} \frac{e^{-S} S^m}{m!} \exp\left[-\frac{(-\Delta E_{LE-CT} + \lambda + m\hbar\omega)^2}{4\lambda kT} \right]$$

where V is the electronic coupling, λ the reorganization energy, $h\omega$ is the vibrational energy and S the Huang–Rhys factor. This expression illustrates how the charge transfer rate depends on three key parameters that is, electronic coupling, reorganization energy, and the LE-CT offset. Within the normal region of MLJ theory ($\lambda > \Delta E_{LE-CT}$) reducing the energy offset decreases the charge transfer rate and can lead to insufficient charge generation. This has been verified for many fullerene and non-fullerene acceptor systems; hence the LE-CT offset has become an important parameter understanding charge generation.

While the MLJ framework is widely used to describe charge-transfer and charge-separation kinetics, it also provides a thermodynamic foundation for understanding voltage losses in OSCs. Using Marcus theory within the detailed balance picture, open-circuit voltage can be expressed as [84]:

$$V_{OC} = \frac{E_{CT}}{q} + \frac{kT}{q} \ln\left(\frac{J_{SC} h^3 c^2}{f q 2\pi (E_{CT} - \lambda)} \right) + \frac{kT}{q} \ln\left(EQE_{EL} \right)$$

here, h is Planck's constant, c is the speed of light, f is the oscillator strength, and λ is the reorganization energy.

The first term represents the fundamental thermodynamic limit to the open-circuit voltage and is directly determined by the CT state energy. The second term accounts for radiative voltage loss, and the third term corresponds to non-radiative voltage loss. In an ideal solar cell, the CT state energy (E_{CT}) dictates the maximum achievable V_{OC}. Since the CT state often serves as the primary recombination channel, especially in systems where excitons on the donor or acceptor rapidly relax into the CT manifold—the energy of the CT state is central to determining voltage losses. Critically, non-radiative voltage loss has been reported to depend on the CT-ground state energy gap. Both theoretical [21] and experimental studies have demonstrated that increasing the CT-state energy (i.e., reducing the energy gap between the LE and CT states) leads to lower non-radiative voltage losses and, consequently, a higher V_{OC} [85]. Hence, the LE-CT energy offset dictates the fundamental thermodynamic limit for V_{OC} and is the key determinant in minimizing voltage losses.

In both the limiting and optimal case, where the LE-CT offset approaches zero, recombination is expected to (partly) occur via the LE states of the low-bandgap component—typically the acceptor. This scenario is relevant for state-of-the-art high-efficiency OSCs, which are progressively moving toward such small-offset regimes. As a result, the luminescence of the blend becomes increasingly governed by the intrinsic emission properties of the neat low-bandgap material and highlighting the critical importance of optimizing the PLQY of the neat materials [85–87].

3 | Techniques to Measure the HOMO and LUMO Level to Quantify the Electronic Offset

To measure the FMO levels in organic semiconductors, electrochemical techniques (like cyclic voltammetry; CV), ultraviolet photoelectron spectroscopy (UPS), and inverse photoemission spectroscopy (IPES) are frequently used. Additionally, spectroelectrochemical (SEC), energy-resolved electrochemical impedance spectroscopy (ER–EIS), and photoemission yield spectroscopy in air (PYSA) have also been recently employed. However, significant discrepancies exist among the values obtained from these various techniques. Figure 1 shows the HOMO-offset (IE-offset) values obtained by CV, SEC and UPS measurements for the benchmark PM6:Y6 system (measured on neat PM6 and Y6 films) by different research groups. The reported offset values vary over a wide range, between 0.08 to 0.26 eV [60, 69],0.34 eV and 0.44 to 0.80 eV [72, 75], respectively for CV, SEC and UPS. Such variability arises because each technique probes different physical processes and does not necessarily provide a direct measurement of the HOMO level. In addition, material-specific factors—such as the choice of solvent (e.g., chloroform versus chlorobenzene), which influence molecular orientation, film morphology, and intermolecular interactions—can further contribute to this spread. This is especially true for materials such as Y6, whose energetics strongly depend on the processing conditions [71]. This highlights the critical need for careful consideration of both the measurement methodology and the processing conditions before drawing conclusions from reported offset values.

3.1 | Electrochemical Method

CV is an electrochemical technique used to measure the FMO levels of the material where varying potential leads to injecting or removing the electron from the material via redox reactions at the electrode-material interface. The resulting current response reflects the electron transfer processes between the organic material and the electrode, thereby allowing the determination of HOMO and/or LUMO levels [88]. Importantly, CV does not directly measure vacuum-referenced energy levels; instead, it reports redox energetics defined within an electrochemical environment. In the CV setup, there are three electrodes (working electrode, reference electrode, and counter electrode) dipped in to an electrolyte solution. The material is deposited on the working electrode, while the reference electrode provides a stable

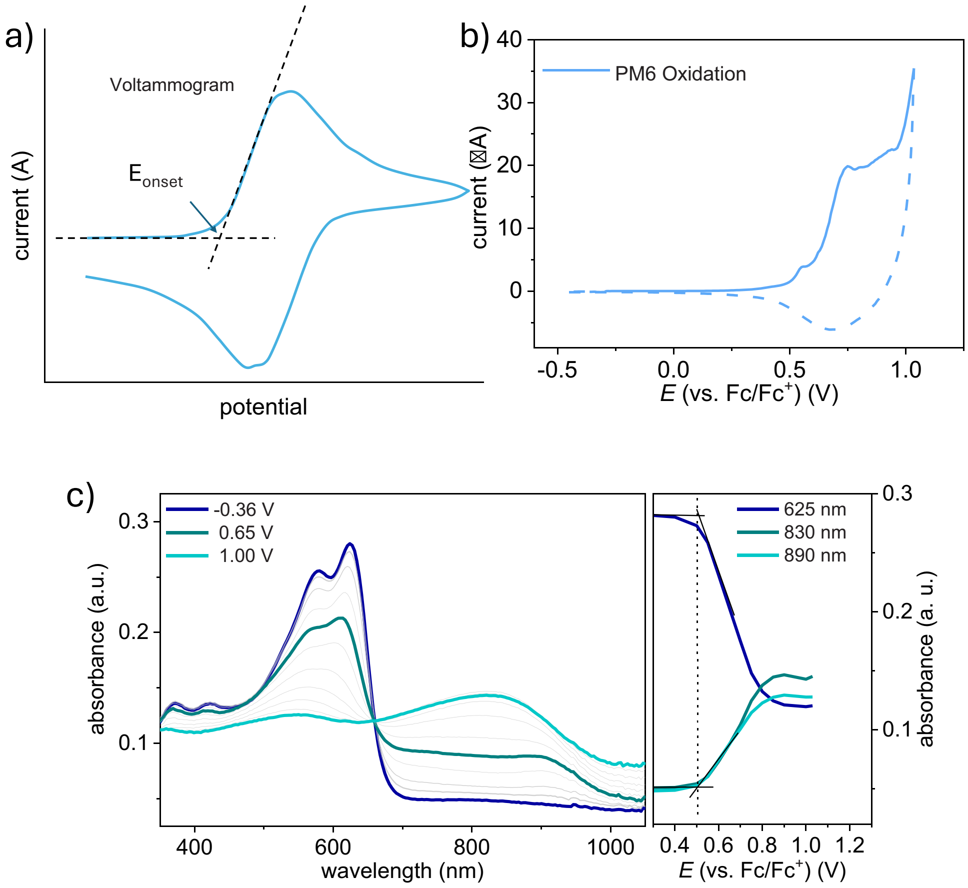

FIGURE 3 | (a) A typical voltammogram CV curve used to extract the onset potential (E_{onset}), (b) Voltammogram oxidation CV curve for pure PM6, which shows a very broad redox wave (multiple redox peak), (c) In situ CV measurement coupled with absorption spectroscopy; the absorption spectra with respect to different oxidation potential shows different absorption features. The peak at different spectral signatures is then plotted against the oxidation potential to determine the onset potential by using tangents. Reproduced with permission from ref. [81] Copyright 2022, Royal Society of Chemistry.

reference potential and a counter electrode completes the circuit [89, 90]. The electrolyte serves a key role by maintaining ionic conductivity and screening the electric field—ensuring that the potential throughout the solution is uniform and referenced to the reference electrode. This enables precise control and measurement of the redox potentials. A positive (to remove an electron from the HOMO) or a negative (to add the electron in the LUMO) linear bias is swept between the working electrode and counter electrode, and the current response of the material can be noted which arises due to redox reaction at the working electrode/material interface. The resulting graph between the current response and applied bias is also known as voltammogram [91]. In CV, the onset energy is typically determined by extrapolating the linear portion of the oxidation current curve to the baseline. The point where this extrapolated tangent intersects the baseline is defined as the onset potential or onset energy, which corresponds to the energy at which oxidation begins to occur (Figure 3a). The measured onset energy is then converted into HOMO or LUMO energy levels. This conversion is typically achieved by calibrating the system against a known internal reference standard—most commonly the ferrocene/ferrocenium (Fc/Fc$^+$) redox couple—which is then correlated to the vacuum level [92]. Further, this onset does not correspond to the peak of the density of states (DOS); rather, it reflects the low-energy tail of the DOS distribution. In disordered organic semiconductor films, the first states accessed during oxidation or reduction are these tail states that are most easily oxidized or reduced molecular sites. The onset potential is therefore a probe of the DOS tail rather than the HOMO or LUMO center.

The onset potential value in CV is important as it decides the position of the HOMO and LUMO level; however, the determination of the onset value has no thermodynamic basis [93]. When interpreting CV data for organic semiconductors, it is important to recognize that the classical electrochemical framework is based on reversible, diffusion-controlled redox reactions in dilute solution which does not directly translate to thin-film measurements. In ideal solution systems, redox species diffuse freely, electron transfer is rapid, and Nernstian equilibrium is readily established at the electrode interface, enabling reliable extraction of oxidation and reduction potentials. In contrast, for solid-state or thin-film CV, these assumptions break down. Redox processes are often governed by slow ion penetration into the organic layer, film swelling upon charge compensation, and structural relaxation of molecular aggregates. These effects lead to quasi-reversible or even irreversible behavior, broad redox features, and significant shifts in onset potential and renders standard Nernstian analysis and the Randles-Sevcik equation inapplicable [92, 94–96]. Therefore, thin film CV often reflects a convolution of charge-transfer kinetics, ion insertion dynamics, and morphological changes rather than the intrinsic electronic energy levels of the material.

In addition, the onset values can be influenced by many factors. 1) It depends on the electrolyte solution used, as it is influenced by the ionic environment and electrolyte conductivity [97, 98]. Moreover, alternative electrolyte solutions interact differently with the material which can alter the ion movement during the redox or oxidation reaction and will affect the onset potential. 2) The scan rate at which the CV is performed can influence the recorded current [99]. When scanning too fast, ions have insufficient time to diffuse into the film, which significantly affects the shape of the voltammogram. 3) The background current, which arises from capacitive charging of the electrode, can obscure the true onset potential. Capacitive currents (a non-Faradaic current) result from the charging and discharging of the electrical double layer that forms at the electrode surface as the applied potential is scanned. This background effects can lead to a gradual rather than sharp rise in current, making it challenging to precisely determine the point at which oxidation or reduction truly begins [96]. 4) The uncertainty in the absolute potential of the reference electrode across different media can introduce significant errors. Often, the energetic scale is based on calculations that neglect solvent and, supporting electrolyte effects, which further complicates the accuracy of the measurements [94]. 5) The broad redox waves in conjugated polymer like PM6 makes it difficult to unambiguously determine an onset value as shown in Figure 3b.

To mitigate some of these problems, square-wave voltammetry (SWV) was introduced [100, 101]. Instead of a linear sweep, SWV applies a series of square wave potential pulses superimposed on a staircase potential. Each cycle consists of a forward pulse and reverse pulse and the difference between them is recorded, cancelling out the background capacitive current. As a result, SWV produces sharp and well-defined peaks at redox potentials and hence facilitates a more precise determination of HOMO and LUMO levels. This method has been shown to predict the V_{OC} quite well for the diketopyrrolopyrrole (DPP) based polymer:fullerene blends [102].

Further, ER-EIS has been introduced as a technique [103], that integrates electrochemical impedance spectroscopy with DC potential gating to map electronic structures over a wide energy range [104]. In this approach, a small AC perturbation is superimposed on a DC voltage sweep, and the resulting impedance response is analyzed at a fixed frequency where redox processes dominate. Specifically, the charge-transfer resistance at the electrolyte/semiconductor interface is extracted to determine the surface density of states (DOS), while the space-charge capacitance can be used to map the bulk DOS. Unlike conventional CV or SWV, which are often limited to determining onset energy level—ER-EIS provides a meticulous map of the entire DOS distribution—enabling the characterization of effective HOMO and LUMO levels, tail states, and the energetic disorder associated with the material's electronic landscape [105, 106].

However, with the continuous emergence of new organic molecules—each exhibiting different solubility and structural properties—standardization of experimental conditions such as the choice of electrolyte or scan rate remains impractical in electrochemical measurements. Further, the presence of the electrolyte and electrode surrounding the organic molecules influences the redox potential in CV, SWV, and ER-EIS measurements [102]. Hence, it will introduce potential errors when comparing the results from different labs.

As a further expansion of the electrochemical techniques, the combination of CV and absorption spectroscopy has been introduced which is also known as spectroelectrochemical (SEC) measurement [81, 107]. This approach leverages the spectroscopic response arising from the applied electrochemical potential, enabling a more detailed analysis of the electronic structure of the material. SEC probes the intermediate charged states (polaron absorption) generated upon electrochemical doping of a thin film. The onset of polaron formation provides an estimate of HOMO and LUMO in the thin film under a controlled potential. Since each charged species exhibits a distinct spectral signature (Figure 3c), this method allows for a more accurate determination of the onset potential (Figure 3d). Specifically, it helps disentangle multiple oxidation steps, thereby providing a clearer and more precise estimation of energy levels. By correlating the onset of polaron absorption with the onset of current flow in CV, SEC pinpoints the actual filling of DOS-tail states rather than relying solely on the electrochemical current, which can be influenced by capacitive or diffusion-related artifacts. As a result, the combination of CV and in situ absorption spectroscopy offers a more reliable interpretation of FMO energy levels compared to conventional CV measurements.

An advantage of SEC measurements is their ability to determine HOMO and LUMO levels directly within donor-acceptor (D:A) blends, as donors and acceptors typically exhibit distinct absorption signatures. Using this method, Neusser et al. calculated the offset between PM6 and Y6, reporting a value of 0.32 eV, which suggests that conventional CV tends to underestimate offset values [81]. However, when the spectral features of the donor and acceptor are indistinguishable- either due to a small energetic offset or very similar bandgaps-this method may not yield reliable results for D:A blends. Nonetheless, compared to conventional CV, SEC measurements provide a more physically meaningful approach for measuring HOMO and LUMO levels, particularly in complex material systems.

Despite these challenges in electrochemical methods, when offset values are measured within the same laboratory under identical conditions for a comparable set of systems, electrochemical techniques like CV and SWV offer a reasonable basis for relative comparison. However, caution must be exercised when drawing conclusions from such data, as these offset values should not be directly extrapolated for comparisons with results obtained from different laboratories, where variations in experimental setups may lead to discrepancies.

3.2 | UPS and IPES

UPS and IPES are two complementary techniques for determining both the frontier energy levels (HOMO, LUMO) and electronic structures of materials, with UPS probing occupied states and IE, and IPES revealing unoccupied states and EA. UPS

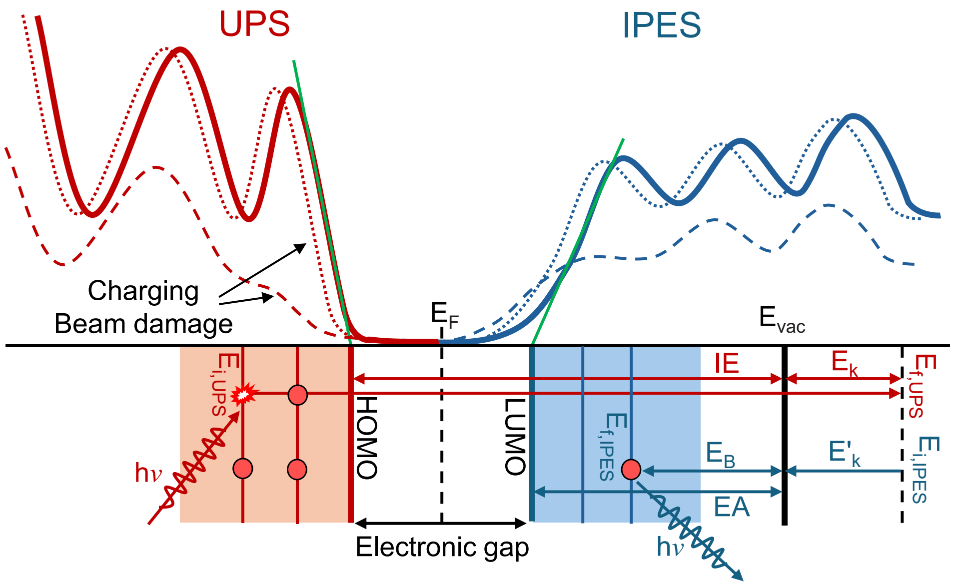

FIGURE 4 | A representation of the working principle of UPS and IPES to measure the IE and EA and hence the HOMO and LUMO levels, respectively.

operates on the photoelectric effect, as illustrated in Figure 4, when a material is irradiated with ultraviolet (UV) light, electrons from occupied electronic states are emitted. The kinetic energy (E_k) of these emitted electrons is measured, and the binding energy (E_B) of the electrons relative to the vacuum level is determined using the energy conservation law: $E_B = h\nu - E_k$. Conversely, in IPES, the sample is exposed to a low-energy electron beam [108]. When an electron is absorbed by the material it falls into an unoccupied state, emitting a photon with energy $h\nu$. By detecting these photons, the energies of unoccupied states and hence the EA can be determined using the same energy conservation law as UPS: $E_B = h\nu - E'_k$, where E_B is taken as a positive value, representing the binding energy of the unoccupied state that captures the electron.

UPS/IPES probes the electronic structure on an ultrafast timescale, allowing only electronic relaxation while geometric relaxation does not have time to occur (the nuclei remain fixed). As a result, UPS/IPES measures the vertical ionization energies rather than the fully relaxed (adiabatic) values. However, it still provides a reliable estimation of material's IE/EA, because electronic relaxation dominates the polarization energy while geometric relaxation contributes only minor shifts. At the same time, it can probe absolute energy levels referenced to the vacuum (and Fermi) level. From UPS/IPES, the band structures can be obtained, allowing access to the density of tail states and interfacial broadening. In contrast, the CV measurements are referenced to a standard electrode and require a conversion to the vacuum energy scale. Additionally, UPS and IPES operate in ultra-high vacuum (UHV), eliminating interference from electrolytes or solvents and minimizing contamination from ambient impurities. This ensures more reliable and reproducible results for solid films [56]. Further, UPS and IPES are highly surface-sensitive (~2 nm). This makes them ideal for analyzing homogeneous thin films but also means that they can be influenced by surface-induced variations, as molecules at the surface may exhibit different ionization energies due to changes in intermolecular relaxation and local environment [109].

Although IE/EA is typically obtained by extrapolating the linear portion of the leading edge in the UPS/IPES spectrum to the baseline (Figure 4), alternative approaches such as logarithmic fitting or Gaussian line-shape fitting—can introduce systematic variations and lead to discrepancies in the extracted energy values. The energy resolution achieved in UPS/IPES measurements is another important factor influencing the determination of IE and EA. Typical energy resolutions are ~50 meV for UPS and ~400 meV for IPES [110–112]. The resolution of IPES can be improved to ~250 meV by using low-energy inverse photoemission spectroscopy (LEIPS) [113], enabling EA determination with uncertainties of approximately 100 meV. Discrepancies in energy-level determination can also arise from common experimental errors, including sample charging, beam damage, instrument miscalibration, etc [114]. Sample charging occurs when excess charge accumulates on a sample during measurement, leading to spectral shifts, peak broadening, or distortion. This typically results from low sample conductivity, poor electrical contact, or high-intensity photon exposure. Beam-induced damage can further smear the electronic structure and broaden spectral features, which can be mitigated by using a low-dose or low-energy beam [115]. Instrument miscalibration is another critical issue that requires aligning the energy scale with a well-characterized metal surface with a known Fermi level (E_F), such as an argon-ion sputter-cleaned gold surface [116].

In addition to energy-resolved techniques such as UPS and IPES, which probe occupied and unoccupied states under UHV conditions, PYSA [117–119], also referred to as photoemission (photoelectron) spectroscopy in air (PESA), has gained increasing attention due to its capability for rapid, high-throughput measurements under ambient conditions. Unlike UPS, PYSA measures the total photoemission yield as a function of photon energy rather than the kinetic energy distribution of emitted electrons. In typical implementations, a tunable deep-UV light source (~3–7 eV) is used to scan photon energy, while the emitted charge, often dominated by atmospheric ions, is collected without energy resolution. The ionization energy is then extracted from the threshold behavior of the yield using power-law transformations (e.g., square-root or cube-root) and linear extrapolation [120]. While experimentally convenient, this approach relies on implicit assumptions, particularly that the measured yield reflects the integrated density of occupied states near the valence band edge. However, low-energy photon excitation can introduce additional contributions such as anion states and biphotonic electron emission [121], and ambient conditions further involve processes including electron scattering, ion formation, surface adsorption, and charge trapping. These factors can influence both the spectral shape and the apparent onset. Consequently, although PYSA offers practical advantages, including ambient operation, minimal sample preparation, and relatively large probing depth, its limited energy range, lack of energy resolution, and indirect yield-based analysis constrain its ability to provide detailed or unambiguous electronic structure information. It is therefore best regarded as a convenient and approximate method for estimating ionization energies, rather than a direct substitute for energy-resolved techniques such as UPS.

Beyond instrumental factors, sample-related effects can also contribute to measurement discrepancies in both electrochemical and UPS/IPES. These include surface contamination from oxidation or adsorbates, variations in morphology due to different sample preparation methods (e.g., solvent selection for film coating [71], post-treatment such as thermal annealing [122]), sample homogeneity issues such as surface roughness, film coverage and batch to batch variation of the materials [123]. These variations are commonly observed in the literature and often lead to discrepancies in reported HOMO and LUMO values obtained from UPS, IPES and electrochemical measurements. Further, at the molecular level, the observed HOMO/LUMO energies are affected by the local environment, for example, surrounding molecules screen the charges created upon redox reactions. In thin films and devices, mesoscale factors such as interfacial electrostatic shifts, molecular packing, structural disorder and (local) permittivity affect the measured IE and EA. Consequently, the experimentally determined energy levels reflect not only the inherent properties of the molecules but also their broader environment and the ways in which they interact with neighboring molecules, interfaces, and the probing method.

Accordingly, it is important to note that HOMO level or LUMO level values at the D:A interface could be very different from the values within neat material phases due to interfacial disorder, electrostatic dipole (vacuum level shift), band-bending [57] and molecules orientation [71]. This implies that the offset calculated by measuring the HOMO and LUMO levels of neat material may not fully capture the actual conditions at the D:A interface. For example, certain crystalline organic semiconductors exhibit orientation-dependent IE/EA values due to molecular quadrupole effects [124], and these levels can be further tuned when materials with different quadrupole moments are intermixed on the molecular scale [125]. Another important consideration when comparing HOMO/LUMO offsets is the mode of energy level alignment between the donor and acceptor. Assuming a strict vacuum level alignment can be misleading, as vacuum level shifts—often caused by interface dipoles that equilibrate chemical-potential differences—commonly occur at interfaces [126, 127]. Recent studies have demonstrated that such interfacial dipoles are prevalent at the D:A interfaces of numerous donor-acceptor combinations, as revealed by UPS measurements that map energy level alignment monolayer by monolayer at well-defined D:A interfaces [128]. While the intrinsic IE/EA values remain largely unchanged, the resulting vacuum level shifts significantly modulate the interfacial energy level offsets—typically reducing the HOMO/LUMO offsets and increasing the photovoltaic gap (the energy difference between the donor HOMO and acceptor LUMO). Thus, when interpreting or comparing energetic offset values, it is essential to distinguish whether they refer to the intrinsic IE/EA differences of isolated neat materials or to the actual energetics that manifest at the real D:A interface.

Further, the numerical discrepancies observed among CV, UPS/IPES, and SEC arise because each technique probes a fundamentally different physical phenomenon and therefore samples different parts of the electronic energy landscape. UPS/IPES measure single-particle ionization and affinity levels at the film–vacuum interface, where molecular packing, surface dipoles, and reduced polarization can modify the HOMO/LUMO energies compared to the bulk film values. Conversely, CV and SEC probe redox processes within the electrolyte-film environment and are influenced by ion diffusion, film swelling, dielectric screening, and morphology-dependent stabilization of charged species. Meanwhile, SEC provides optical signatures of polarons generated within the bulk of the blend, where local disorder and interfacial dielectric heterogeneity further modify the effective energy levels. Because these techniques probe different electronic states, environments, and degrees of dielectric stabilization, it is expected and unavoidable that the extracted offsets vary, sometimes substantially, even for the same donor-acceptor system. This same origin of variation also explains the long-recognized differences between electronic bandgaps extracted from CV and UPS/IPES [56]. Recognizing the origin of these differences is therefore essential for interpreting energetic offsets in OSCs.

Similar to the CV method, the energy levels determined using UPS and IPES can be reliably compared when measurements are conducted under identical conditions. However, direct comparisons with values reported in the literature without accounting for these potential differences in sample preparation and measurement conditions, can be problematic.

In Figure 5, we summarized the IE-offset values determined by SEC and UPS for various D:A systems, alongside their corresponding free charge generation efficiencies (CGE). Here, the CGE is estimated as the ratio of the measured short-circuit current density (J_{SC}) to the Shockley-Queisser limit J_{SC} (J_{SQ}), where J_{SQ} is calculated assuming an external quantum efficiency of 100% for all photon energies above the bandgap. While this represents a simplified approximation of CGE, it is nonetheless effective in capturing the influence of the energetic offset on charge generation behavior. The IE-offset values included in Figure 5b are determined from the IE differences between neat donor and acceptor films measured via UPS; crucially, all were measured in the same laboratory under consistent experimental conditions, thereby avoiding discrepancies arising from

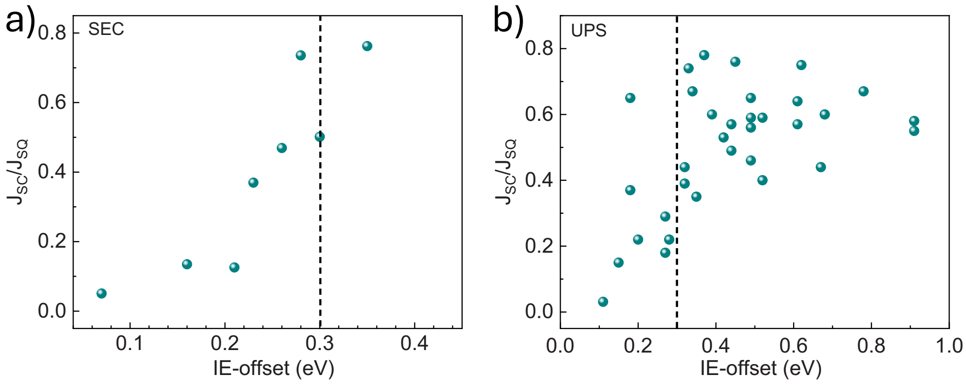

FIGURE 5 | Charge generation efficiency vs the IE-offset calculated by the (a) spectroelectrochemical method [107] (for blend systems) and (b) UPS measurement for number of D:A systems (Here the IE values obtained from the UPS for all the samples are measured in the same lab and for the neat donor and acceptor: Table S2).

lab-to-lab variations. From Figure 5, it is evident that CGE is strongly influenced by the IE-offset, with efficiency decreasing as the IE-offset decreases below 0.3 eV. Both SEC and UPS measurements provide a similar trade-off limit for the offset with charge generation.

While UPS has been widely employed across many NFA systems to determine energy levels, SEC methods have not been utilized as extensively for offset measurements. As a result, there are relatively few data points available to include in Figure 5a (Here it is worth noting that these values were measured in blend). This underutilization is likely due to limited awareness of the method's advantages and its relatively lower accessibility in many research groups. In this perspective, we strongly encourage broader adoption of SEC techniques, especially for high-efficiency NFA systems—as they offer significant benefits over conventional CV-based approaches for accurately determining energetic offsets.

Furthermore, previous studies reported IE-offset thresholds of 0.5 eV [56, 57] (measured via UPS), our analysis (Figure 5b) suggests a lower threshold of 0.3 eV. This discrepancy stems from the instrumental and methodological limitations discussed earlier. A deeper understanding of this issue is complicated by the variability in literature-reported IE-offset values, which, if incorporated into Figure 5b, would introduce significant ambiguity. For instance, in the case of PM6:Y6, reported IE-offset values (measured on neat PM6 and Y6) vary widely across different studies—ranging from 0.44 to 0.80 eV—highlighting the challenges associated with cross-laboratory comparisons.

4 | Techniques to Calculate the CT State Energy to Quantify the Excitonic Offset

A CT state formed in a mixed D:A system with a large energetic offset shows a very distinct sub-gap absorption [129, 131]. For instance, in the poly[2-methoxy-5-(3,7-dimethyloctyloxy)-1,4-phenylenevinylene:Phenyl-C61-butyric acid methyl ester (MDMO-PPV:PCBM) system (Figure 6a), the absorption spectrum extends down to 1.1 eV, whereas the individual donor and acceptor materials exhibit absorption down to 1.6 eV. This indicates that the absorption feature below 1.6 eV is associated with CT state absorption. However, CT states typically have a much lower oscillator strength than the donor or acceptor singlet states and cannot be visualized using regular UV–vis absorption spectroscopy. The CT state absorption feature can be visualized by more sensitive techniques to measure the sub-gap absorption spectrum, such as photothermal deflection spectroscopy (PDS) which has the sensitivity to measure absorption down to magnitudes of 10^{-3}–10^{-4} (Figure 6a) [131, 132]. Another way to measure the CT state absorption is to measure the photocurrent response (external quantum efficiency, EQE) using Fourier transform photocurrent spectroscopy (FTPS), which measures the photocurrent down to a magnitude of 10^{-5}–10^{-6} (Figure 6b) [84, 133]. FTPS is widely utilized in literature as it has more sensitivity than PDS and can be applied directly to photovoltaic devices.

Within the framework of Marcus theory, Vandewal et al. presented a formula to determine the CT state energy (E_{CT}) [84]. This formula can be used to fit the FTPS spectra in regimes where the CT state absorption can be differentiated from both the donor and acceptor absorption regions. The low energy part of the CT state absorption region can be fitted using the following equation:

$$EQE_{PV}(E) \propto \frac{1}{E\sqrt{4\pi\lambda kT}}exp\left(\frac{-(E_{CT}+\lambda-E)^2}{4\lambda kT}\right) \qquad (1)$$

where E is the photon energy, kT is the thermal energy, λ is the reorganization energy and E_{CT} is the CT state energy. The electroluminescence (EL) spectrum can be fitted with an equivalent equation, that is,

$$EL(E) \propto \frac{1}{E\sqrt{4\pi\lambda kT}}exp\left(\frac{-(E_{CT}-\lambda-E)^2}{4\lambda kT}\right) \qquad (2)$$

An example of MDMO-PPV:PCBM is shown in Figure 6b. First, the reduced EQE (EQE(E) × E) is fitted with Equation 1 and the parameters are extracted, including E_{CT}. Extracted parameters are then used to regenerate the EL spectra by using Equation 2, with good agreement with the experimental data. This verifies the reliability to use this method to calculate the real CT state energy in the D:A complex. This method has been widely used in the community to calculate the CT state energy of fullerene-based OSCs at room temperature [84, 130, 134–138].

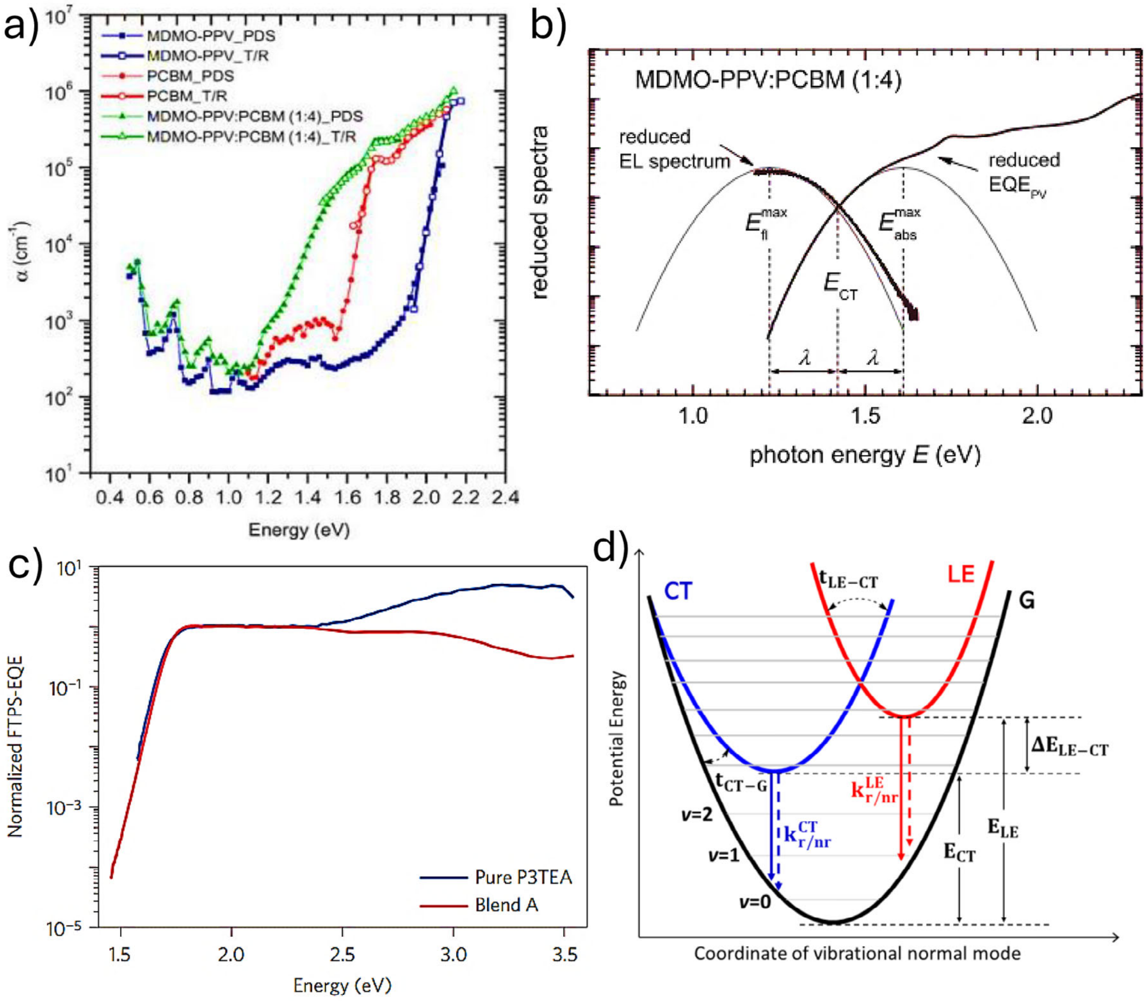

FIGURE 6 | (a) Photothermal spectroscopy data for pure MDMO-PPV, PCBM and MDMO-PPV:PCVBM. Reproduced with permission from ref [129]. Copyright 2005, Springer Nature. (b) FTPS EQE (reduced EQE) spectra and EL spectra for MDMO-PPV:PCBM. The spectra are fitted with the Marcus equation 1 and 2. Reproduced with permission from ref. [84] Copyright 2010, American Physical Society. (c) FTPS EQE spectra for pure P3TEA and blend P3TEA:SF-PDI$_2$ system; Reproduced with permission from ref. [130] Copyright 2016, Springer Nature. (d) Schematic illustration of the potential energy surfaces for the ground state (G), charge-transfer (CT) state, and local excitonic (LE) diabatic states; where $t_{\text{LE-CT}}$ and $t_{\text{CT-G}}$ represents the electronic coupling of the LE with CT state and CT with ground state, respectively. Reproduced with permission from ref [85] Copyright 2021, Springer Nature.

Now, to calculate the LE-CT energetic offset, it is essential to reliably determine the optical bandgap of the blend system. In our previous work, we discussed several methods for estimating the optical bandgap [139]. In this perspective article, we employ the derivative of the EQE spectrum of the blend to extract the optical bandgap [139]; the difference between the bandgap energy and the CT state energy provides the offset. Therefore, both the low bandgap energy (Eg) and CT state energy (E_{CT}) can be determined exclusively by using EQE spectra. The primary advantage of this method over the FMO methods is that it measures the E_{CT} in the device, thereby yielding highly reliable values and mitigating lab-to-lab variations.

However, state-of-the-art, high-efficiency D:A blends do not exhibit clearly distinguishable CT absorption in their EQE spectra (or CT emission in EL spectra); rather, the CT state absorption merges with the LE state absorption of the material, as shown in Figure 6c [39, 51, 55]. Therefore, the method described above, although well suited for conventional fullerene based OSCs, cannot be reliably applied to determine the CT state energy in high efficiency NFA based OSCs.

We, with other colleagues, developed the three-state model (Figure 6d) and applied it to the EL spectra of numerous NFA-based D:A blends. By utilizing the fitting parameters derived from this model, the CT state energy of these blends can be accurately determined [85]. In the model, the role of thermal population and hybridization of the states on the recombination is explored using the coupling between ground state, LE state and CT state. It has been noted that both hybridization and thermal population affect the CT state recombination. When the offset is low, thermal population between the LE and CT plays an important role. At room temperature —there is strong thermal population between the CT state and the LE state—resulting in emission dominating by the LE state and making the CT state invisible. The emission or the EQE can be fitted with the three-state dynamic vibronic model

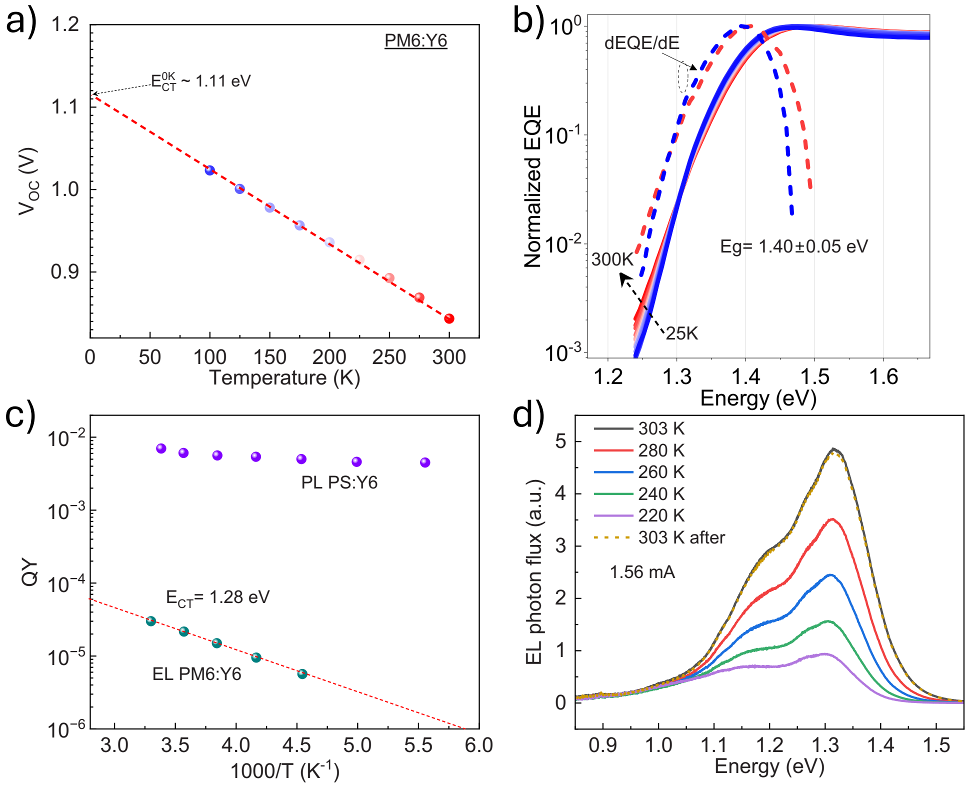

FIGURE 7 | (a) V_{OC}-T measurement for PM6:Y6 and linearly extrapolated to T = 0 K to extract the charge-transfer state energy. (b) temperature dependent external quantum efficiency measurement for PM6:Y6 to show that the bandgap of the system is independent of the temperature, where the dashed line shows the derivative of the EQE spectra. Reproduced with permission from ref [51]. as per the Creative Commons license CC-BY-4.0; (c) temperature dependent luminescence intensity; PL for PS:Y6 and EL for PM6:Y6 normalized to the room temperature PLQY and ELQY value; and (d) temperature dependent EL spectra to show that the shape of the EL spectra remains the same throughout the measured temperature range. Reproduced with permission from ref [142]. Copyright 2021, American Chemical Society.

to obtain the energy of the CT state as described in Equation 3. The accuracy of the fitting values is usually within the range of 100 meV.

$$I_e\ (E) = E^3 \sum_{\alpha} f\left(E_\alpha\right) \sum_{m,n} \mathrm{I} \left\langle \Psi_{hybrid;\alpha}\ \mathrm{I}\, \vec{\mu}\, \mathrm{I}\ \Psi_{G;m,n} \right\rangle \mathrm{I}^2 \delta \left(E - \left(E_\alpha - E_{m,n}\right)\right) \tag{3}$$

here, $I_e(E)$ is the optical emission intensity per D:A pair, $f(E_\alpha)$ is the thermal population of the vibronic state, E_α,$E_{m,n}$ are the total energies of all the vibrational normal modes, and $\mathrm{I}\langle\Psi_{hybrid;\alpha}\ \mathrm{I}\,\vec{\mu}\,\mathrm{I}\ \Psi_{G;m,n}\rangle\mathrm{I}^2$ is the transition dipole moment of each hybrid vibronic state (more detail of the model and code is available in reference [85]). While the value of CT state energy, along with other parameters obtained from Equation 3, is informative, comparing energetic offsets across different systems remains challenging due to an inherent uncertainty of ~100 meV in low-offset regimes, where the LE and CT emissions cannot be spectrally resolved even at low temperatures. This limitation becomes particularly significant when the LE and CT states lie very close in energy—typically within 100 meV—such that even temperature-dependent measurements fail to resolve them as separate features.

An alternative method would be to use temperature-dependent V_{OC} measurements. Based on the Marcus framework, Vandewal et al. measured the temperature-dependent CT state energy (using Equation 1 & 2) in fullerene-based systems and linearly extrapolated the data to T = 0 K. They found that the CT state energy at 0 K matches well with the open circuit voltage at T = 0 K [84]. Hence the lower lying CT state energy can also be determined using the temperature-dependent V_{OC} measurements. Further, while disorder and dark leakage currents can affect the V_{OC} at low temperatures, utilizing linear interpolation in the higher temperature range allows for a reliable estimation of the CT state energy at 0 K [140, 141].

As an example, V_{OC}-T measurement for PM6:Y6 has been performed by a several research groups, and the extrapolated value of Voc at 0 K was consistently determined to be around 1.11 eV (Figure 7a) [40, 51, 86, 143]. Given that the optical bandgap of PM6:Y6 is 1.4 eV (similar for different temperatures; Figure 7b), the driving force, or the offset, for the charge generation is approximately 0.29 eV. This highlights two points: 1) The variation in the offset values typically observed with other methods like CV or UPS, can be avoided by the temperature dependent V_{OC} measurements. 2) The offset value obtained via this method is measured in the device; hence, it provides a reasonable estimation of the excess energy at the D:A interface. Here it is worth noting that this method measures the CT state energy at 0 K and hence

TABLE 1 | Key methods to determine the LE-CT offsets: Probed quantities, advantages, and limitations.

Method	What it probes	Advantage	Limitations
Marcus charge transfer model	Fits the sensitive absorption, photo-current or EL of the blend	1. Physically well-grounded model. 2. Reciprocity relation holds. 3. Works very well for fullerene-based systems or when LE-CT offset ≥ 0.2 eV.	Accuracy limited when LE-CT offset < ~200 meV
Three-state model	Fits the sensitive absorption, photo-current or EL of the blend	1. Considers the hybridization and thermal population between the LE and CT states. 2. Valid for both fullerene and non-fullerene systems as long as LE and CT emissions or absorption can be spectrally resolved either at room temp or low temp.	Accuracy limited when LE-CT offset < 100 meV
Temperature-dependent V_{OC} (V_{OC}-T)	Device V_{OC} as a function of temperature	1. Simple and device-relevant method. 2. Directly probes the V_{OC}. 3. Applicable to all types of system including the multicomponent system.	Provides CT energy at 0 K, not at RT
Temperature-dependent ELQY (ELQY-T)	Radiative recombination efficiency as a function of temperature	1. Sensitive to calculate the LE-CT energy gap even if it is very low.	Requires temperature independent PLQY, CT decay rate and EL shape

overestimates the offset (underestimates the CT state energy) value at room temperature (RT).

Recently, temperature dependent electroluminescence quantum yield (ELQY-T) measurements have been introduced to calculate the precise energetic offset in systems where the emission originates predominantly from the LE state of the low bandgap component (in low offset systems only) [107, 142, 144, 145]. In such cases, the EL spectrum reflects repopulated LE excitons formed via back-transfer from the CT states. By monitoring how the ELQY changes with temperature under constant current injection, the energy difference (ΔE) between the CT and LE states can be extracted using Equation 4.

$$ELQY\,(T) = ELQY_{\infty} \times exp^{-\frac{\Delta E}{kT}} \tag{4}$$

here $ELQY_{\infty}$ is the infinite temperature ELQY, and ΔE corresponds to the energetic offset that is, the difference between the LE state energy (Eg) and CT state energy (E_{CT}). For example, in PM6:Y6 systems, this method yields an offset of approximately ~ 0.12 eV (Figure 7c) [142].

To ensure the reliability of this method, some cautions need to be considered. First, the shape and peak position of the EL spectra needs to remain stable across the fitting temperature range. Any deviation would invalidate the assumption that the emission arises exclusively from the LE state (Figure 7d). Second, the method assumes that the CT decay rate remains largely unaffected by temperature. In current state-of-the-art systems—where emission is dominated by the LE state—it becomes challenging to directly probe the CT decay rate and hence variations in CT decay rate could misinterpret the value of the offset. Third, as vibrational modes are naturally temperature-dependent and can introduce competing non-radiative decay pathways, it's necessary to confirm that the PLQY of the low bandgap component remains the same throughout the temperature range.

Table 1 summarizes the key differences between the major methods used to determine the excitonic offset, highlighting what each technique probes, along with their respective advantages and limitations. This comparison is intended to provide clearer guidance on when each method is reliable.

Figure 8 summarizes the free charge generation efficiency as a function of the LE-CT offset, as determined from V_{OC}-T measurements and ELQY-T measurements for various samples obtained from literature. The data clearly indicates that there is a threshold value for efficient free charge generation; this value is estimated to be around 0.2 eV for the V_{OC}-T measurements and approximately 0.1 eV for the ELQY-T measurements. Although both the V_{OC}-T and ELQY-T measurements offer reasonable estimations of the LE-CT energetic offset, the values they yield can differ significantly. As discussed, these discrepancies arise from the distinct physical processes each method probes. Nevertheless, both techniques hold strong potential for consistent inter-laboratory comparison, as they rely on electro-optical measurements rather than electrochemical references. Further, ELQY-T measurements demand stricter experimental conditions, for instance, stable emission characteristics, and temperature-independent PLQY—which can complicate their implementation. In contrast, V_{OC}-T is more user-friendly, straightforward to implement, and broadly accessible, making it a practical tool for routine offset evaluation across different labs.

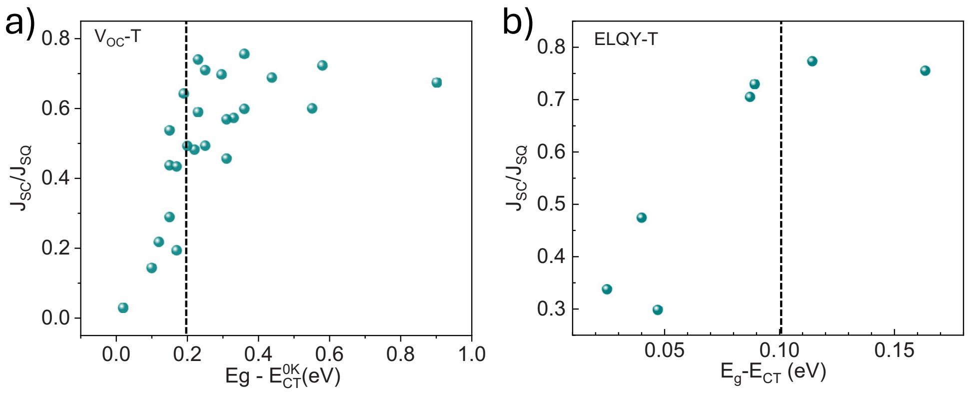

FIGURE 8 | Charge generation efficiency vs the energetic offset calculated by the (a) V_{OC}-T measurement. Reproduced with permission from ref [86]. as per the Creative Commons license CC-BY-4.0 and, (b) ELQY-T measurement for different D:A system [107, 144].

TABLE 2 | Summary of HOMO offsets obtained from neat PM6 and Y6 system using CV, SEC, and UPS, alongside LE-CT offsets extracted from V_{OC}-T and ELQY-T measurements for state-of-the-art PM6:Y6 blend system. For CV and UPS, the listed offset values correspond to the average values of the data presented in Figure 1.

Methods	CV	SEC	UPS	V_{OC}-T	ELQY-T
HOMO offset or LE-CT offset	0.16 eV	0.34 eV	0.56 eV	0.29 eV	0.11 eV

5 | Conclusion

In this perspective, we critically examined the diverse techniques used to determine electronic and excitonic energetic offsets in OSCs. Because each method probes a fundamentally different physical quantity—ranging from single-particle redox processes to interfacial density-of-states tails and excitonic energetics—the offset values reported in the literature often span a wide range even for the same donor–acceptor pair as summarized in Table 2 for PM6:Y6 system. Such discrepancies arise not only from intrinsic differences in the materials themselves (neat vs blend) but also from the assumptions and limitations inherent to each technique. Overall, no single technique universally provides the “correct” energy offset. Instead, each method contributes complementary information, and therefore careful consideration of its assumptions, sensitivities, and limitations is vital.

Further, to obtain reliable estimations of the energetic offsets and to properly understand the fundamentals of charge generation and voltage loss, it is advisable to rely on temperature-dependent electro-optical techniques—such as Voc-T and ELQY-T measurements—for determining the LE-CT offset. Importantly, these measurements promote cross-laboratory consistency, enabling offset values to be compared reliably and reproducibly across different research environments. These methods offer the distinct advantage of being applicable to both multicomponent systems (e.g., ternary or quaternary blends) and single-component OSCs, wherein donor and acceptor units are covalently linked. However, when comparing a particular set of systems synthesized and studied within the same lab, it remains appropriate to use other methods, such as CV, SWV, SEC and UPS. These methods have the advantage that they can be applied on thin films of neat donor and acceptor, before devices are fabricated.

The primary motivation for reducing the energetic offset between the donor and acceptor is to minimize non-radiative voltage losses and enhance the Voc. As a result, the precise numerical value of this offset is less critical than the overall reduction in voltage loss. In this context, understanding the physical significance of offsets determined via different methodologies holds greater value than attempting to define a single offset value, given that these experimental values are often not directly comparable. However, reliably defining and quantifying the offset remains crucial when the primary focus is to understand the fundamentals of the charge carrier generation. Until such mechanistic insights become the focus, voltage loss remains a more practical and comparable parameter across different studies, making it a more meaningful benchmark for OSC performance.

6 | Outlook

To further advance the OSC field, voltage losses need to be minimized below 0.4 eV, while the current state-of-the-art systems have a voltage loss of ~0.5 eV (Figure 9a). The main loss component in these systems other than the fundamental loss is the non-radiative loss which stands close to 0.16 eV in NFA OSCs while perovskite solar cells exhibit non-radiative losses around 0.06 eV. The value of ~0.16 eV in state-of-the-art OSCs has now saturated in the last few years without any significant improvement. The main reason for this saturation is the intrinsic limit of the state-of-the-art acceptor materials we are currently using.

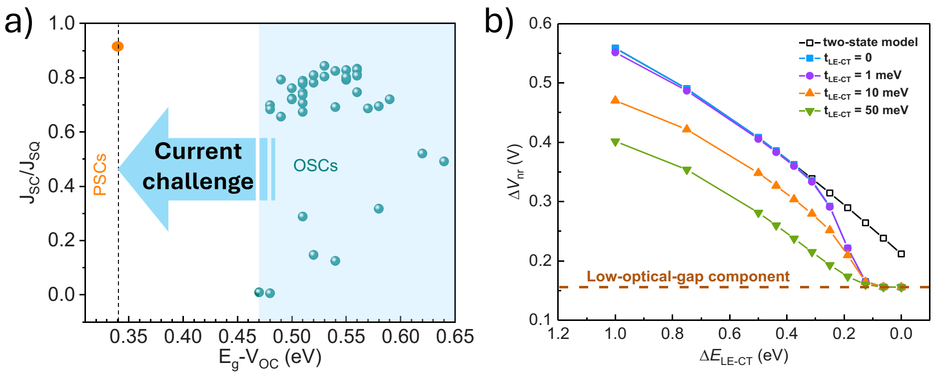

FIGURE 9 | (a) Voltage loss vs the free charge generation efficiency for various D:A systems (Table S3), (the orange circle represents the CGE value for efficient perovskite solar cell), (b) Calculated ΔVnr using the three-state model as a function of offset. Different colors represent varying LE-CT coupling strengths, increasing from 1 to 50 meV from top to bottom. The brown dashed lines indicate the luminescence quantum yield of the low bandgap component. Enhancing the PLQY of the low bandgap component further reduces the lowest value achievable for ΔVnr. Reproduced with permission from ref. [85] Copyright 2021, Springer Nature.

Our previous findings on non-radiative losses highlight that its intrinsic limit fundamentally depends on the quantum yield of the low bandgap component material [85, 86]. The study indicates that when the charge-transfer state energy and local excitonic states are close to each other, CT states thermally populate the LE state at room temperature. This means that the radiative recombination is ultimately determined by the quantum yield of the low bandgap component. For donor-acceptor systems with low energetic offset, the emission quantum yield and non-radiative decay rate of the blend are determined by the intrinsic emission properties of the low bandgap material, thereby establishing the intrinsic limit for V_{OC}. We emphasize that it is not necessary to have a 'zero' offset for recombination to be governed by the low-bandgap component; rather, thermal population effects allow this condition to be realized even in the presence of a finite energetic offset (Figure 9b).

The current state-of-the-art NFAs typically exhibit ELQY values in the range of 0.1% to 0.3% [147]. Notably, several blends—such as PTO2:Y6, PMTT56:FOIC, PM6:Y11, and PDCBT-2F:IT-M/ITIC—display non-radiative losses of 0.16–0.20 eV, which are consistent with the intrinsic values of the neat acceptors [85, 148–150]. These examples corroborate the concept that in such systems, the quantum yield of the pristine NFA establishes the practical limit for the device Voc. Therefore, to push non-radiative voltage losses below 0.1 eV, the rational design and development of novel molecules with inherently higher emission quantum yields is essential.

Acknowledgements

The authors thank Prof. Dieter Neher for his valuable feedback. The authors also thank Prof. Alexander J. Gillett, David Hardy and Dr. Huotian Zhang for insightful discussions. The authors acknowledge the financial support received from the Swedish Research Council VR (2022-04902 and 2024–02081), Göran Gustafsson Prize to F.G., and the Swedish Government Strategic Research Area in Materials Science on Functional Materials at Linköping University (faculty grant number SFO-Mat-LiU #2009-00971). Xian'e Li thanks the Swedish research council (2023-00357) for financial support. O.I. and F.G. are Wallenberg Scholars.

Conflicts of Interest

The authors declare no conflict of interest.

References

1. L. Wang, C. Chen, Z. Gan, et al., "Diluted Ternary Heterojunctions to Suppress Charge Recombination for Organic Solar Cells With 21% Efficiency," *Advanced Materials* 37 (2025): 1–8, https://doi.org/10.1002/adma.202419923.

2. Y. Jiang, K. Liu, F. Liu, et al., "20.6% Efficiency Organic Solar Cells Enabled by Incorporating a Lower Bandgap Guest Nonfullerene Acceptor Without Open-Circuit Voltage Loss," *Advanced Materials* 37 (2025): 2500282, https://doi.org/10.1002/adma.202500282.

3. X. Song, B. Zhang, X. Liu, et al., "Low-Volatility Fused-Ring Solid Additive Engineering for Synergistically Elongating Exciton Lifetime and Mitigating Trap Density Toward Organic Solar Cells of 20.5% Efficiency," *Advanced Materials* 37 (2025): 2418393, https://doi.org/10.1002/adma.202418393.

4. H. Chen, Y. Huang, R. Zhang, et al., "Organic Solar Cells With 20.82% Efficiency and High Tolerance of Active Layer Thickness Through Crystallization Sequence Manipulation," *Nature Materials* 24 (2025): 444–453, https://doi.org/10.1038/s41563-024-02062-0.

5. C. Li, J. Song, H. Lai, et al., "Non-Fullerene Acceptors With High Crystallinity and Photoluminescence Quantum Yield Enable >20% Efficiency Organic Solar Cells," *Nature Materials* 24 (2025): 433–443, https://doi.org/10.1038/s41563-024-02087-5.

6. Z. Chen, J. Ge, W. Song, et al., "20.2% Efficiency Organic Photovoltaics Employing a π-Extension Quinoxaline-Based Acceptor With Ordered Arrangement," *Advanced Materials* 36 (2024): 2406690, https://doi.org/10.1002/adma.202406690.

7. L. Zhu, M. Zhang, G. Zhou, et al., "Achieving 20.8% Organic Solar Cells via Additive-Assisted Layer-by-Layer Fabrication With Bulk p-i-n Structure and Improved Optical Management," *Joule* 8 (2024): 3153–3168, https://doi.org/10.1016/j.joule.2024.08.001.

8. J. Hou, O. Inganas, R. H. Friend, and F. Gao, "Organic Solar Cells Based on Non-Fullerene Acceptors," *Nature Materials* 17 (2018): 119–128, https://doi.org/10.1038/NMAT5063.

9. J. Wang, Y. Xie, K. Chen, H. Wu, J. M. Hodgkiss, and X. Zhan, "Physical Insights Into Non-Fullerene Organic Photovoltaics," *Nature Reviews Physics* 6 (2024): 365–381, https://doi.org/10.1038/s42254-024-00719-y.

10. J. Zhao, Y. Li, G. Yang, et al., "Efficient Organic Solar Cells Processed From Hydrocarbon Solvents," *Nature Energy* 1 (2016): 15027, https://doi.org/10.1038/NENERGY.2015.27.

11. M. C. Scharber, “On the Efficiency Limit of Conjugated Polymer:Fullerene-Based Bulk Heterojunction Solar Cells,” *Advanced Materials* 28 (2016): 1994–2001, https://doi.org/10.1002/adma.201504914.

12. W. Li, K. H. Hendriks, A. Furlan, M. M. Wienk, and R. A. J. Janssen, “High Quantum Efficiencies in Polymer Solar Cells at Energy Losses Below 0.6 eV,” *Journal of the American Chemical Society* 137 (2015): 2231–2234, https://doi.org/10.1021/ja5131897.

13. Y. Cai, H. Zhang, L. Ye, et al., “Effect of the Energy Offset on the Charge Dynamics in Nonfullerene Organic Solar Cells,” *ACS Applied Materials & Interfaces* 12 (2020): 43984–43991, https://doi.org/10.1021/acsami.0c13085.

14. A. Jungbluth, E. Cho, A. Privitera, et al., “Limiting Factors for Charge Generation in Low-Offset Fullerene-Based Organic Solar Cells,” *Nature Communications* 15 (2024): 2302452, https://doi.org/10.1038/s41467-024-49432-5.

15. M. A. Faist, T. Kirchartz, W. Gong, et al., “Competition Between the Charge Transfer State and the Singlet States of Donor or Acceptor Limiting the Efficiency in Polymer: Fullerene Solar Cells,” *Journal of the American Chemical Society* 134 (2012): 685–692, https://doi.org/10.1021/ja210029w.

16. J. L. Brédas, D. Beljonne, V. Coropceanu, and J. Cornil, “Charge-Transfer and Energy-Transfer Processes in π-Conjugated Oligomers and Polymers: A Molecular Picture,” *Chemical Reviews* 104 (2004): 4971–5004, https://doi.org/10.1021/cr040084k.

17. M. C. Scharber, D. Mühlbacher, M. Koppe, et al., “Design Rules for Donors in Bulk-Heterojunction Solar Cells—Towards 10 % Energy-Conversion Efficiency,” *Advanced Materials* 18 (2006): 789–794, https://doi.org/10.1002/adma.200501717.

18. A. J. Ward, A. Ruseckas, M. M. Kareem, et al., “The Impact of Driving Force on Electron Transfer Rates in Photovoltaic Donor–Acceptor Blends,” *Advanced Materials* 27 (2015): 2496–2500, https://doi.org/10.1002/adma.201405623.

19. T. M. Clarke and J. R. Durrant, “Charge Photogeneration in Organic Solar Cells,” *Chemical Reviews* 110 (2010): 6736–6767, https://doi.org/10.1021/cr900271s.

20. G. Wen, R. Hu, J. Feng, et al., “Energy Level Offsets Determine the Interplay Between Charge and Energy Transfer in All-Small-Molecule Organic Solar Cells,” *Chemical Engineering Journal* 475 (2023): 145939, https://doi.org/10.1016/j.cej.2023.145939.

21. M. Azzouzi, J. Yan, T. Kirchartz, et al., “Nonradiative Energy Losses in Bulk-Heterojunction Organic Photovoltaics,” *Physical Review X* 8 (2018): 31055, https://doi.org/10.1103/PhysRevX.8.031055.

22. T. Saito, S. ichiro Natsuda, K. Imakita, Y. Tamai, and H. Ohkita, “Role of Energy Offset in Nonradiative Voltage Loss in Organic Solar Cells,” *Solar RRL* 4 (2020): 2000255, https://doi.org/10.1002/solr.202000255.

23. J. Benduhn, K. Tvingstedt, F. Piersimoni, et al., “Intrinsic Non-radiative Voltage Losses in Fullerene-Based Organic Solar Cells,” *Nature Energy* 2 (2017): 17053, https://doi.org/10.1038/nenergy.2017.53.

24. R. Shivhare, T. Erdmann, U. Hörmann, et al., “Alkyl Branching Position in Diketopyrrolopyrrole Polymers: Interplay Between Fibrillar Morphology and Crystallinity and Their Effect on Photogeneration and Recombination in Bulk-Heterojunction Solar Cells,” *Chemistry of Materials* 30 (2018): 6801–6809, https://doi.org/10.1021/acs.chemmater.8b02739.

25. N. A. Ran, J. A. Love, C. J. Takacs, et al., “Harvesting the Full Potential of Photons With Organic Solar Cells,” *Advanced Materials* 28 (2016): 1482–1488, https://doi.org/10.1002/adma.201504417.

26. C. Wang, X. Xu, W. Zhang, et al., “Low Band Gap Polymer Solar Cells with Minimal Voltage Losses,” *Advanced Energy Materials* 6 (2016): 1–10, https://doi.org/10.1002/aenm.201600148.

27. K. Kawashima, Y. Tamai, H. Ohkita, I. Osaka, and K. Takimiya, “High-Efficiency Polymer Solar Cells With Small Photon Energy Loss,” *Nature Communications* 6 (2015): 10085, https://doi.org/10.1038/ncomms10085.

28. C. Sun, S. Qin, R. Wang, et al., “High Efficiency Polymer Solar Cells With Efficient Hole Transfer at Zero Highest Occupied Molecular Orbital Offset Between Methylated Polymer Donor and Brominated Acceptor,” *Journal of the American Chemical Society* 142 (2020): 1465–1474, https://doi.org/10.1021/jacs.9b09939.

29. X. Li, X. Li, M. A. Pan, et al., “Roles of Acceptor Guests in Tuning the Organic Solar Cell Property Based on an Efficient Binary Material System With a Nearly Zero Hole-Transfer Driving Force,” *Chemistry of Materials* 32 (2020): 5182–5191, https://doi.org/10.1021/acs.chemmater.0c01245.

30. Y. Liu, J. Zhang, G. Zhou, F. Liu, X. Zhu, and F. Zhang, “Electric Field Facilitating Hole Transfer in Non-Fullerene Organic Solar Cells With a Negative HOMO Offset,” *The Journal of Physical Chemistry C* 124 (2020): 15132–15139, https://doi.org/10.1021/acs.jpcc.0c05654.

31. W. Li, S. Zeiske, O. J. Sandberg, D. B. Riley, P. Meredith, and A. Armin, “Organic Solar Cells With near-unity Charge Generation Yield,” *Energy & Environmental Science* 14 (2021): 6484–6493, https://doi.org/10.1039/d1ee01367j.

32. S. Li, L. Zhan, C. Sun, et al., “Highly Efficient Fullerene-Free Organic Solar Cells Operate at near Zero Highest Occupied Molecular Orbital Offsets,” *Journal of the American Chemical Society* 141 (2019): 3073–3082, https://doi.org/10.1021/jacs.8b12126.

33. L. Wang, C. Zhang, Z. Su, et al., “Near 0 eV HOMO Offset Enable High-performance Nonfullerene Organic Solar Cells With Large Open Circuit Voltage and Fill Factor,” *Journal of Materials Chemistry C* 11 (2023): 6971–6980, https://doi.org/10.1039/d3tc00547j.

34. S. Wang, Y. Tao, S. Li, et al., “A Benzobis(thiazole)-Based Wide Bandgap Polymer Donor Enables Over 15% Efficiency Organic Photovoltaics With a Flat Energetic Offset,” *Macromolecules* 54 (2021): 7862–7869, https://doi.org/10.1021/acs.macromol.1c01301.

35. S. Li, L. Zhan, T. K. Lau, et al., “Near-Infrared Nonfullerene Acceptors Based on Benzobis(thiazole) Unit for Efficient Organic Solar Cells With Low Energy Loss,” *Small Methods* 3 (2019): 1900531, https://doi.org/10.1002/smtd.201900531.

36. S. Ma, S. Wu, J. Zhang, et al., “Heptacyclic S,N-Heteroacene-Based Near-Infrared Nonfullerene Acceptor Enables High-Performance Organic Solar Cells With Small Highest Occupied Molecular Orbital Offsets,” *ACS Applied Materials & Interfaces* 12 (2020): 51776–51784, https://doi.org/10.1021/acsami.0c19033.

37. Z. Zhou, W. Liu, G. Zhou, et al., “Subtle Molecular Tailoring Induces Significant Morphology Optimization Enabling Over 16% Efficiency Organic Solar Cells With Efficient Charge Generation,” *Advanced Materials* 32 (2020): 1906324, https://doi.org/10.1002/adma.201906324.

38. D. Baran, T. Kirchartz, S. Wheeler, et al., “Reduced Voltage Losses Yield 10% Efficient Fullerene Free Organic Solar Cells With >1 V Open Circuit Voltages,” *Energy & Environmental Science* 9 (2016): 3783–3793, https://doi.org/10.1039/c6ee02598f.

39. S. Chen, Y. Wang, L. Zhang, et al., “Efficient Nonfullerene Organic Solar Cells With Small Driving Forces for both Hole and Electron Transfer,” *Advanced Materials* 30 (2018): 1804215, https://doi.org/10.1002/adma.201804215.

40. P. Wan, X. Chen, Q. Liu, et al., “Direct Observation of the Charge Transfer States From a Non-Fullerene Organic Solar Cell With a Small Driving Force,” *The Journal of Physical Chemistry Letters* 12 (2021): 10595–10602, https://doi.org/10.1021/acs.jpclett.1c03365.

41. X. Zhu, “The Critical Isomerization Effect of Core Bromination on Nonfullerene Acceptors in Achieving High-Performance Organic Solar Cells With Low Energy Loss,” *Advanced Materials* 37 (2025): 2413376, https://doi.org/10.1002/adma.202413376.

42. R. Wang, C. Zhang, Q. Li, Z. Zhang, X. Wang, and M. Xiao, “Charge Separation From an Intra-Moiety Intermediate State in the High-Performance PM6:Y6 Organic Photovoltaic Blend,” *Journal of the American Chemical Society* 142 (2020): 12751–12759, https://doi.org/10.1021/jacs.0c04890.

43. L. Ma, H. Yao, J. Wang, et al., "Impact of Electrostatic Interaction on Bulk Morphology in Efficient Donor–Acceptor Photovoltaic Blends," *Angewandte Chemie International Edition* 60 (2021): 15988–15994, https://doi.org/10.1002/anie.202102622.

44. G. Zhou, M. Zhang, Z. Chen, et al., "Marcus Hole Transfer Governs Charge Generation and Device Operation in Nonfullerene Organic Solar Cells," *ACS Energy Letters* 6 (2021): 2971–2981, https://doi.org/10.1021/acsenergylett.1c01154.

45. M. B. Price, P. A. Hume, A. Ilina, et al., "Free Charge Photogeneration in a Single Component High Photovoltaic Efficiency Organic Semiconductor," *Nature Communications* 13 (2022): 2827, https://doi.org/10.1038/s41467-022-30127-8.

46. L. Zhu, J. Zhang, Y. Guo, C. Yang, Y. Yi, and Z. Wei, "Small Exciton Binding Energies Enabling Direct Charge Photogeneration Towards Low-Driving-Force Organic Solar Cells," *Angewandte Chemie* 133 (2021): 15476–15481, https://doi.org/10.1002/ange.202105156.

47. C. He, Y. Pan, Y. Ouyang, et al., "Manipulating the D:A Interfacial Energetics and Intermolecular Packing for 19.2% Efficiency Organic Photovoltaics," *Energy & Environmental Science* 15 (2022): 2537–2544, https://doi.org/10.1039/d2ee00595f.

48. H. Yao, D. Qian, H. Zhang, et al., "Critical Role of Molecular Electrostatic Potential on Charge Generation in Organic Solar Cells," *Chinese Journal of Chemistry* 36 (2018): 491–494, https://doi.org/10.1002/cjoc.201800015.

49. S. I. Natsuda, T. Saito, R. Shirouchi, et al., "Cascaded Energy Landscape as a Key Driver for Slow yet Efficient Charge Separation With Small Energy Offset in Organic Solar Cells," *Energy & Environmental Science* 15 (2022): 1545–1555, https://doi.org/10.1039/d1ee03565g.

50. T. F. Hinrichsen, C. C. S. Chan, C. Ma, et al., "Long-lived and Disorder-free Charge Transfer States Enable Endothermic Charge Separation in Efficient Non-fullerene Organic Solar Cells," *Nature Communications* 11 (2020): 1–10, https://doi.org/10.1038/s41467-020-19332-5.

51. L. Perdigón-Toro, H. Zhang, A. Markina, et al., "Barrierless Free Charge Generation in the High-Performance PM6:Y6 Bulk Heterojunction Non-Fullerene Solar Cell," *Advanced Materials* 32 (2020): 1906763, https://doi.org/10.1002/adma.201906763.

52. D. Balzer and I. Kassal, "Delocalisation Enables Efficient Charge Generation in Organic Photovoltaics, Even With Little to no Energetic Offset," *Chemical Science* 15 (2024): 4779–4789, https://doi.org/10.1039/d3sc05409h.

53. S. M. Menke, A. Cheminal, P. Conaghan, et al., "Order Enables Efficient Electron-Hole Separation at an Organic Heterojunction With a Small Energy Loss," *Nature Communications* 9 (2018): 277, https://doi.org/10.1038/s41467-017-02457-5.

54. T. F. Hinrichsen, C. C. S. Chan, C. Ma, et al., "Long-lived and Disorder-free Charge Transfer States Enable Endothermic Charge Separation in Efficient Non-Fullerene Organic Solar Cells," *Nature Communications* 11 (2020): 5617, https://doi.org/10.1038/s41467-020-19332-5.

55. A. Classen, C. L. Chochos, L. Lüer, et al., "The Role of Exciton Lifetime for Charge Generation in Organic Solar Cells at Negligible Energy-level Offsets," *Nature Energy* 5 (2020): 711–719, https://doi.org/10.1038/s41560-020-00684-7.

56. J. Bertrandie, J. Han, C. S. P. De Castro, et al., "The Energy Level Conundrum of Organic Semiconductors in Solar Cells," *Advanced Materials* 34 (2022): 2202575, https://doi.org/10.1002/adma.202202575.

57. S. Karuthedath, J. Gorenflot, Y. Firdaus, et al., "Intrinsic Efficiency Limits in Low-Bandgap Non-Fullerene Acceptor Organic Solar Cells," *Nature Materials* 20 (2021): 378–384, https://doi.org/10.1038/s41563-020-00835-x.

58. J. Yuan, Y. Zhang, L. Zhou, et al., "Single-Junction Organic Solar Cell With Over 15% Efficiency Using Fused-Ring Acceptor With Electron-Deficient Core," *Joule* 3 (2019): 1140–1151, https://doi.org/10.1016/j.joule.2019.01.004.

59. X. Chen, Q. Zhang, D. Wang, et al., "High-Efficiency Ternary Organic Solar Cells Based on the Synergized Polymeric and Small-Molecule Donors," *Solar RRL* 4 (2020): 2000537, https://doi.org/10.1002/solr.202000537.

60. J. Wu, J. Lee, Y. C. Chin, et al., "Exceptionally Low Charge Trapping Enables Highly Efficient Organic Bulk Heterojunction Solar Cells," *Energy & Environmental Science* 13 (2020): 2422–2430, https://doi.org/10.1039/d0ee01338b.

61. Y. Chen, T. Liu, L. K. Ma, et al., "Alkoxy Substitution on IDT-Series and Y-Series Non-Fullerene Acceptors Yielding Highly Efficient Organic Solar Cells," *Journal of Materials Chemistry A* 9 (2021): 7481–7490, https://doi.org/10.1039/d0ta10953c.

62. F. Liu, L. Zhou, W. Liu, et al., "Organic Solar Cells With 18% Efficiency Enabled by an Alloy Acceptor: A Two-in-One Strategy," *Advanced Materials* 33 (2021): 2100830, https://doi.org/10.1002/adma.202100830.

63. J. Song, C. Li, L. Zhu, et al., "Ternary Organic Solar Cells With Efficiency >16.5% Based on Two Compatible Nonfullerene Acceptors," *Advanced Materials* 31 (2019): 1905645, https://doi.org/10.1002/adma.201905645.

64. Y. Tang, J. Yu, H. Sun, et al., "Two Compatible Polymer Donors Enabling Ternary Organic Solar Cells With a Small Nonradiative Energy Loss and Broad Composition Tolerance," *Solar RRL* 4 (2020): 2000396, https://doi.org/10.1002/solr.202000396.

65. L. Xu, W. Tao, H. Liu, et al., "Achieving 17.38% Efficiency of Ternary Organic Solar Cells Enabled by a Large-bandgap Donor With Noncovalent Conformational Locking," *Journal of Materials Chemistry A* 9 (2021): 11734–11740, https://doi.org/10.1039/d1ta02075g.

66. T. Yan, W. Song, J. Huang, R. Peng, L. Huang, and Z. Ge, "16.67% Rigid and 14.06% Flexible Organic Solar Cells Enabled by Ternary Heterojunction Strategy," *Advanced Materials* 31 (2019): 1902210, https://doi.org/10.1002/adma.201902210.

67. Q. Ma, Z. Jia, L. Meng, et al., "Promoting Charge Separation Resulting in Ternary Organic Solar Cells Efficiency Over 17.5%," *Nano Energy* 78 (2020): 105272, https://doi.org/10.1016/j.nanoen.2020.105272.

68. Q. An, J. Wang, X. Ma, et al., "Two Compatible Polymer Donors Contribute Synergistically for Ternary Organic Solar Cells With 17.53% Efficiency," *Energy & Environmental Science* 13 (2020): 5039–5047, https://doi.org/10.1039/d0ee02516j.

69. M. A. Pan, T. K. Lau, Y. Tang, et al., "16.7%-Efficiency Ternary Blended Organic Photovoltaic Cells With PCBM as the Acceptor Additive to Increase the Open-Circuit Voltage and Phase Purity," *Journal of Materials Chemistry A* 7 (2019): 20713–20722, https://doi.org/10.1039/c9ta06929a.

70. W. Tang, W. Peng, M. Zhu, et al., "17.25% High Efficiency Ternary Solar Cells With Increased Open-Circuit Voltage Using a High HOMO Level Small Molecule Guest Donor in a PM6:Y6 Blend," *Journal of Materials Chemistry A* 9 (2021): 20493–20501, https://doi.org/10.1039/d1ta05284e.

71. Y. Fu, T. H. Lee, Y. C. Chin, et al., "Molecular Orientation-Dependent Energetic Shifts in Solution-Processed Non-Fullerene Acceptors and Their Impact on Organic Photovoltaic Performance," *Nature Communications* 14 (2023): 1870, https://doi.org/10.1038/s41467-023-37234-0.

72. S. Liang, S. Li, Y. Zhang, et al., "Efficient Hole Transfer via Delocalized Excited State in Small Molecular Acceptor: A Comparative Study on Photodynamics of PM6:Y6 and PM6:ITIC Organic Photovoltaic Blends," *Advanced Functional Materials* 31 (2021): 2102764, https://doi.org/10.1002/adfm.202102764.

73. M. Zhang, L. Zhu, G. Zhou, et al., "Single-Layered Organic Photovoltaics With Double Cascading Charge Transport Pathways: 18% Efficiencies," *Nature Communications* 12 (2021): 309, https://doi.org/10.1038/s41467-020-20580-8.

74. L. Bai, S. Chung, Z. Zhao, et al., "Modulating Acceptor Phase Leads to 19.59% Efficiency Organic Solar Cells," *Advanced Science* 12 (2024): 2413051, https://doi.org/10.1002/advs.202413051.

75. J. Kosco, S. Gonzalez-Carrero, C. T. Howells, et al., "Generation of Long-lived Charges in Organic Semiconductor Heterojunction Nanoparticles for Efficient Photocatalytic Hydrogen Evolution," *Nature Energy* 7 (2022): 340–351, https://doi.org/10.1038/s41560-022-00990-2.

76. X. Y. Zhu, "How to Draw Energy Level Diagrams in Excitonic Solar Cells," *The Journal of Physical Chemistry Letters* 5 (2014): 2283–2288, https://doi.org/10.1021/jz5008438.

77. J. L. Bredas, "Mind the gap!," *Materials Horizon* 1 (2014): 17–19, https://doi.org/10.1039/c3mh00098b.

78. X. Li, *Interfaces in Organic Solar Cells* (Linköping University, Faculty of Science & Engineering, 2023), https://doi.org/10.3384/9789180751292.

79. A. Jablonski, "Efficiency of Anti-Stokes Fluorescence in Dyes," *Nature* 131 (1933): 839–840, https://doi.org/10.1038/131839b0.

80. R. Šípoš and J. Šima, "Jablonski Diagram Revisited," *Revista Cubana De Fisica* 37 (2020): 125–130.

81. D. Neusser, B. Sun, W. L. Tan, et al., "Spectroelectrochemically Determined Energy Levels of PM6:Y6 Blends and Their Relevance to Solar Cell Performance," *Journal of Materials Chemistry C* 10 (2022): 11565–11578, https://doi.org/10.1039/d2tc01918c.

82. K. Vandewal, "Interfacial Charge Transfer States in Condensed Phase Systems," *Annual Review of Physical Chemistry* 67 (2016): 113–133, https://doi.org/10.1146/annurev-physchem-040215-112144.

83. S. R. Forrest, *Charge Transport in Organic Semiconductors* (Oxford Academic, 2020): 171–292, https://doi.org/10.1093/oso/9780198529729.003.0004.

84. K. Vandewal, K. Tvingstedt, A. Gadisa, O. Inganäs, and J. V. Manca, "Relating the Open-circuit Voltage to Interface Molecular Properties of Donor:Acceptor Bulk Heterojunction Solar Cells," *Physical Review B* 81 (2010): 125204, https://doi.org/10.1103/PhysRevB.81.125204.

85. X.-K. Chen, D. Qian, Y. Wang, et al., "A Unified Description of Non-radiative Voltage Losses in Organic Solar Cells," *Nature Energy* 6 (2021): 799–806, https://doi.org/10.1038/s41560-021-00843-4.

86. N. Jain, R. Jasiūnas, X. Li, et al., "The Role of Thermally Activated Charge Separation in Organic Solar Cells," *Advanced Energy Materials* 16 (2024): 1–7, https://doi.org/10.1002/aenm.202403675.

87. W. Liu, J. Yuan, Y. Nai, et al., "Conformationally Locked Macrocyclic Acceptors With Enhanced Photoluminescence for High-Efficiency Organic Solar Cells," *Advanced Materials* n/a (2025): 19607, https://doi.org/10.1002/adma.202519607.

88. D. T. Pierce and W. E. Geiger, "Electrochemical Kinetic Discrimination of the Single-Electron-Transfer Events of a Two-Electron-Transfer Reaction: Cyclic Voltammetry of the Reduction of the Bis(hexamethylbenzene)Ruthenium Dication," *Journal of the American Chemical Society* 114 (1992): 6063–6073, https://doi.org/10.1021/ja00041a026.

89. J. F. Rusling and S. L. Suib, "Characterizing Materials With Cyclic Voltammetry," *Advanced Materials* 6 (1994): 922–930, https://doi.org/10.1002/adma.19940061204.

90. F. Harnisch and S. Freguia, "A Basic Tutorial on Cyclic Voltammetry for the Investigation of Electroactive Microbial Biofilms," *Chemistry—An Asian Journal* 7 (2012): 466–475, https://doi.org/10.1002/asia.201100740.

91. C. J. Tonzola, M. M. Alam, W. Kaminsky, and S. A. Jenekhe, "New n-Type Organic Semiconductors: Synthesis, Single Crystal Structures, Cyclic Voltammetry, Photophysics, Electron Transport, and Electroluminescence of a Series of Diphenylanthrazolines," *Journal of the American Chemical Society* 125 (2003): 13548–13558, https://doi.org/10.1021/ja036314e.

92. N. Elgrishi, K. J. Rountree, B. D. McCarthy, E. S. Rountree, T. T. Eisenhart, and J. L. Dempsey, "A Practical Beginner's Guide to Cyclic Voltammetry," *Journal of Chemical Education* 95 (2018): 197–206, https://doi.org/10.1021/acs.jchemed.7b00361.

93. K. Bruchlos, D. Trefz, A. Hamidi-Sakr, et al., "Poly(3-hexylthiophene) Revisited—Influence of Film Deposition on the Electrochemical Behaviour and Energy Levels," *Electrochimica Acta* 269 (2018): 299–311, https://doi.org/10.1016/j.electacta.2018.02.126.

94. C. M. Cardona, W. Li, A. E. Kaifer, D. Stockdale, and G. C. Bazan, "Electrochemical Considerations for Determining Absolute Frontier Orbital Energy Levels of Conjugated Polymers for Solar Cell Applications," *Advanced Materials* 23 (2011): 2367–2371, https://doi.org/10.1002/adma.201004554.

95. B. A. Frontana-uribe and S. Ludwigs, "Electrochemistry of Conducting Polymers s Persistent Models and New," *Chemical Reviews* 8 (2010): 4724–4771.

96. A. J. Bard, L. R. Faulkner, and H. S. White, *Electrochemical Methods: Fundamentals and Applications* (Wiley, 2022).

97. S. B. Khoo, J. K. Foley, and S. Pons, "Electrolyte Effects on the Cyclic Voltammetry of TCNQ and TCNE," *Journal of Electroanalytical Chemistry and Interfacial Electrochemistry* 215 (1986): 273–285, https://doi.org/10.1016/0022-0728(86)87021-8.

98. E. J. F. Dickinson, J. G. Limon-petersen, N. V. Rees, and R. G. Compton, "How Much Supporting Electrolyte Is Required to Make a Cyclic Voltammetry Experiment Quantitatively " Diffusional " A Theoretical and Experimental Investigation," *The Journal of Physical Chemistry C* 113 (2009): 11157–11171, https://doi.org/10.1021/jp901628h.

99. J. J. Van Benschoten, J. Y. Lewis, W. R. Heineman, D. A. Roston, and P. T. Kissinger, "Cyclic Voltammetry Experiment," *Journal of Chemical Education* 60 (1983): 772–776, https://doi.org/10.1021/ed060p772.

100. O. Inganäs, F. Zhang, K. Tvingstedt, L. M. Andersson, S. Hellström, and M. R. Andersson, "Polymer Photovoltaics With Alternating Copolymer/Fullerene Blends and Novel Device Architectures," *Advanced Materials* 22 (2010): E100–E116, https://doi.org/10.1002/adma.200904407.

101. S. Admassie, O. Inganäs, W. Mammo, E. Perzon, and M. R. Andersson, "Electrochemical and Optical Studies of the Band Gaps of Alternating Polyfluorene Copolymers," *Synthetic Metals* 156 (2006): 614–623, https://doi.org/10.1016/j.synthmet.2006.02.013.

102. R. E. M. Willems, C. H. L. Weijtens, X. de Vries, R. Coehoorn, and R. A. J. Janssen, "Relating Frontier Orbital Energies From Voltammetry and Photoelectron Spectroscopy to the Open-Circuit Voltage of Organic Solar Cells," *Advanced Energy Materials* 9 (2019): 1803677, https://doi.org/10.1002/aenm.201803677.

103. V. Nádaždy, F. Schauer, and K. Gmucová, "Energy Resolved Electrochemical Impedance Spectroscopy for Electronic Structure Mapping in Organic Semiconductors," *Applied Physics Letters* 105 (2014): 142109, https://doi.org/10.1063/1.4898068.

104. H. Bässler, D. Kroh, F. Schauer, V. Nádaždy, and A. Köhler, "Mapping the Density of States Distribution of Organic Semiconductors by Employing Energy Resolved–Electrochemical Impedance Spectroscopy," *Advanced Functional Materials* 31 (2021): 2007738, https://doi.org/10.1002/adfm.202007738.

105. D. Kroh, S. Athanasopoulos, V. Nádaždy, F. Kahle, H. Bässler, and A. Köhler, "An Impedance Study of the Density of States Distribution in Blends of PM6:Y6 in Relation to Barrierless Dissociation of CT States," *Advanced Functional Materials* 34 (2024): 2302520, https://doi.org/10.1002/adfm.202302520.

106. K. Gmucová, "Energy-Resolved Electrochemical Impedance Spectroscopy—An Efficient and Powerful Tool for DOS Characterization in Semiconductors," *Small Methods* 10 (2026): 01920, https://doi.org/10.1002/smtd.202501920.

107. M. Pranav, A. Shukla, D. Moser, et al., "On the Critical Competition Between Singlet Exciton Decay and Free Charge Generation in Non-fullerene Based Organic Solar Cells With Low Energetic Offsets," *Energy & Environmental Science* 17 (2024): 6676–6697, https://doi.org/10.1039/d4ee01409j.

108. F. J. Himpsel, “Inverse Photoemission From Semiconductors,” *Surface Science Reports* 12 (1990): 3–48, https://doi.org/10.1016/0167-5729(90)90005-X.

109. W. R. Salaneck, “Intermolecular Relaxation Energies in Anthracene,” *Physical Review Letters* 40 (1978): 60–63, https://doi.org/10.1103/PhysRevLett.40.60.

110. H. Yoshida, “Low-Energy Inverse Photoemission Study on the Electron Affinities of Fullerene Derivatives for Organic Photovoltaic Cells,” *The Journal of Physical Chemistry C* 118 (2014): 24377–24382, https://doi.org/10.1021/jp509141y.

111. H. Yoshida, “Measuring the Electron Affinity of Organic Solids: An Indispensable New Tool for Organic Electronics,” *Analytical and Bioanalytical Chemistry* 406 (2014): 2231–2237, https://doi.org/10.1007/s00216-014-7659-1.

112. H. Yoshida, “Principle and Application of Low Energy Inverse Photoemission Spectroscopy: A New Method for Measuring Unoccupied States of Organic Semiconductors,” *Journal of Electron Spectroscopy and Related Phenomena* 204 (2015): 116–124, https://doi.org/10.1016/j.elspec.2015.07.003.

113. J.-P. Yang, F. Bussolotti, S. Kera, and N. Ueno, “Origin and Role of Gap States in Organic Semiconductor Studied by UPS: As the Nature of Organic Molecular Crystals,” *Journal of Physics D: Applied Physics* 50 (2017): 423002, https://doi.org/10.1088/1361-6463/aa840f.

114. J. E. Whitten, “Ultraviolet Photoelectron Spectroscopy: Practical Aspects and Best Practices,” *Applied Surface Science Advances* 13 (2023): 100384, https://doi.org/10.1016/j.apsadv.2023.100384.

115. H. Wang, M. Oehzelt, S. Winkler, R. Ovsyannikov, N. Koch, and P. Amsalem, “Electronic Properties and Degradation Upon VUV Irradiation of Sodium Chloride on Ag(111) Studied by Photoelectron Spectroscopy,” *Electronic Structure* 3 (2021): 034008, https://doi.org/10.1088/2516-1075/ac2464.

116. G. Greczynski and L. Hultman, “X-ray Photoelectron Spectroscopy: Towards Reliable Binding Energy Referencing,” *Progress in Materials Science* 107 (2020): 100591, https://doi.org/10.1016/j.pmatsci.2019.100591.

117. A. You, M. Be, and I. In, “Externally Quenched Air Counter for Low—Energy Electron Emission Measurements,” *Review Of Scientific Instruments* 70 (1992): 68–70.

118. I. D. Baikie, A. Grain, J. Sutherland, and J. Law, “Near Ambient Pressure Photoemission Spectroscopy of Metal and Semiconductor Surfaces,” *Physica Status Solidi c* 12 (2015): 259–262, https://doi.org/10.1002/pssc.201400086.

119. H. Ishii, H. Kinjo, T. Sato, S. Machida, and Y. Nakayama, *Photoelectron Yield Spectroscopy for Organic Materials and Interfaces BT—Electronic Processes in Organic Electronics: Bridging Nanostructure, Electronic States and Device Properties*, ed. H. Ishii, K. Kudo, T. Nakayama, and N. Ueno, (Springer Japan, 2015), 131–155, https://doi.org/10.1007/978-4-431-55206-2_8.

120. H. Ishii, *Photoelectron Yield Spectroscopy BT—Compendium of Surface and Interface Analysis*, (Springer Singapore, 2018), 457–463, https://doi.org/10.1007/978-981-10-6156-1_75.

121. R. Nakazawa, M. Kitaoka, R. Kaimori, et al., “Determining the Density of in-Gap States in Organic Semiconductors: A Pitfall of Photoelectron Yield Spectroscopy,” *The Journal of Physical Chemistry C* 130 (2026): 3418–3427, https://doi.org/10.1021/acs.jpcc.5c07058.

122. C. Wang, F. Moro, S. Ni, et al., “Thermal-annealing Effects on Energy Level Alignment at Organic Heterojunctions and Corresponding Voltage Losses in All-Polymer Solar Cells,” *Nano Energy* 72 (2020): 104677, https://doi.org/10.1016/j.nanoen.2020.104677.

123. T. Schultz, T. Lenz, N. Kotadiya, et al., “Reliable Work Function Determination of Multicomponent Surfaces and Interfaces: The Role of Electrostatic Potentials in Ultraviolet Photoelectron Spectroscopy,” *Advanced Materials Interfaces* 4 (2017): 1700324, https://doi.org/10.1002/admi.201700324.

124. S. Duhm, G. Heimel, I. Salzmann, et al., “Orientation-dependent Ionization Energies and Interface Dipoles in Ordered Molecular Assemblies,” *Nature Materials* 7 (2008): 326–332, https://doi.org/10.1038/nmat2119.

125. M. Schwarze, W. Tress, B. Beyer, et al., “Band structure engineering in organic semiconductors,” *Science* 352 (2016): 1446–1449, https://doi.org/10.1126/science.aaf0590.

126. M. Fahlman, S. Fabiano, V. Gueskine, D. Simon, M. Berggren, and X. Crispin, “Interfaces in Organic Electronics,” *Nature Reviews Materials* 4 (2019): 627–650, https://doi.org/10.1038/s41578-019-0127-y.

127. X. Li, Q. Zhang, X. Liu, and M. Fahlman, “Pinning Energies of Organic Semiconductors in High-Efficiency Organic Solar Cells,” *Journal of Semiconductors* 44 (2023): 032201, https://doi.org/10.1088/1674-4926/44/3/032201.

128. X. Li, Q. Zhang, J. Yu, et al., “Mapping the Energy Level Alignment at Donor/Acceptor Interfaces in Non-Fullerene Organic Solar Cells,” *Nature Communications* 13 (2022): 2046, https://doi.org/10.1038/s41467-022-29702-w.

129. L. Goris, K. Haenen, M. Nesládek, et al., “Absorption Phenomena in Organic Thin Films for Solar Cell Applications Investigated by Photothermal Deflection Spectroscopy,” *Journal of Materials Science* 40 (2005): 1413–1418, https://doi.org/10.1007/S10853-005-0576-0/METRICS.

130. J. Liu, S. Chen, D. Qian, et al., “Fast Charge Separation in a Non-Fullerene Organic Solar Cell With a Small Driving Force,” *Nature Energy* 1 (2016): 16089, https://doi.org/10.1038/nenergy.2016.89.

131. L. Goris, A. Poruba, L. Hod′Ákova, et al., “Observation of the Subgap Optical Absorption in Polymer-Fullerene Blend Solar Cells,” *Applied Physics Letters* 88 (2006): 052113, https://doi.org/10.1063/1.2171492.

132. J. J. Benson-Smith, L. Goris, K. Vandewal, et al., “Formation of a Ground-State Charge-Transfer Complex in Polyfluorene//[6,6]-Phenyl-C61 Butyric Acid Methyl Ester (PCBM) Blend Films and Its Role in the Function of Polymer/PCBM Solar Cells,” *Advanced Functional Materials* 17 (2007): 451–457, https://doi.org/10.1002/adfm.200600484.

133. K. Vandewal, A. Gadisa, W. D. Oosterbaan, et al., “The Relation Between Open-Circuit Voltage and the Onset of Photocurrent Generation by Charge-Transfer Absorption in Polymer : Fullerene Bulk Heterojunction Solar Cells,” *Advanced Functional Materials* 18 (2008): 2064–2070, https://doi.org/10.1002/adfm.200800056.

134. R. Sharma, N. Jain, H. Lee, D. Kabra, and S. Yoo, “Comprehensive and Comparative Analysis of Photoinduced Charge Generation, Recombination Kinetics, and Energy Losses in Fullerene and Non-fullerene Acceptor-Based Organic Solar Cells,” *ACS Applied Materials & Interfaces* 12 (2020): 45083–45091, https://doi.org/10.1021/acsami.0c13579.

135. N. Jain, N. Chandrasekaran, A. Sadhanala, R. H. Friend, C. R. McNeill, and D. Kabra, “Interfacial Disorder in Efficient Polymer Solar Cells: The Impact of Donor Molecular Structure and Solvent Additives,” *Journal of Materials Chemistry A* 5 (2017): 24749–24757, https://doi.org/10.1039/c7ta07924a.

136. W. Zhao, D. Qian, S. Zhang, et al., “Fullerene-Free Polymer Solar Cells With Over 11% Efficiency and Excellent Thermal Stability,” *Advanced Materials* 28 (2016): 4734–4739, https://doi.org/10.1002/adma.201600281.

137. B. Bernardo, D. Cheyns, B. Verreet, R. D. Schaller, B. P. Rand, and N. C. Giebink, “Delocalization and Dielectric Screening of Charge Transfer States in Organic Photovoltaic Cells,” *Nature Communications* 5 (2014): 3245, https://doi.org/10.1038/ncomms4245.

138. K. Vandewal, S. Albrecht, E. T. Hoke, et al., “Efficient Charge Generation by Relaxed Charge-Transfer States at Organic Interfaces,” *Nature Materials* 13 (2014): 63–68, https://doi.org/10.1038/nmat3807.

139. Y. Wang, D. Qian, Y. Cui, et al., “Optical Gaps of Organic Solar Cells as a Reference for Comparing Voltage Losses,” *Advanced Energy Materials* 8 (2018): 1801352, https://doi.org/10.1002/aenm.201801352.

140. F. Gao, W. Tress, J. Wang, and O. Inganäs, "Temperature Dependence of Charge Carrier Generation in Organic Photovoltaics," *Physical Review Letter* 114 (2015): 128701, https://doi.org/10.1103/PHYSREVLETT.114.128701/SI-R2_.PDF.

141. Y. Tang, J. M. Bjuggren, Z. Fei, M. R. Andersson, M. Heeney, and C. R. McNeill, "Origin of Open-Circuit Voltage Turnover in Organic Solar Cells at Low Temperature," *Solar RRL* 4 (2020); 2000375, https://doi.org/10.1002/SOLR.202000375.

142. L. Perdigón-Toro, L. Q. Phuong, S. Zeiske, et al., "Excitons Dominate the Emission From PM6:Y6 Solar Cells, but This Does Not Help the Open-Circuit Voltage of the Device," *ACS Energy Letters* 6 (2021): 557–564, https://doi.org/10.1021/acsenergylett.0c02572.

143. L. Perdigón-Toro, L. Q. Phuong, F. Eller, et al., "Understanding the Role of Order in Y-Series Non-Fullerene Solar Cells to Realize High Open-Circuit Voltages," *Advanced Energy Materials* 12 (2022): 2103422, https://doi.org/10.1002/aenm.202103422.

144. B. Sun, N. Tokmoldin, O. Alqahtani, et al., "Toward More Efficient Organic Solar Cells: A Detailed Study of Loss Pathway and Its Impact on Overall Device Performance in Low-Offset Organic Solar Cells," *Advanced Energy Materials* 13 (2023): 2300980, https://doi.org/10.1002/aenm.202300980.

145. M. S. Shadabroo, N. Tokmoldin, A. Shukla, et al., "When the Triplet State Doesn't Matter: Insights Into Its Impact on VOC," *ACS Energy Letters* 10 (2025): 2419–2427, https://doi.org/10.1021/acsenergylett.5c00384.

146. C. Li, J. Zhou, J. Song, et al., "Non-fullerene Acceptors With Branched Side Chains and Improved Molecular Packing to Exceed 18% Efficiency in Organic Solar Cells," *Nature Energy* 6 (2021): 605–613, https://doi.org/10.1038/s41560-021-00820-x.

147. Q. Liu and K. Vandewal, "Understanding and Suppressing Non-Radiative Recombination Losses in Non-Fullerene Organic Solar Cells," *Advanced Materials* 35 (2023): 2302452, https://doi.org/10.1002/adma.202302452.

148. S. Liu, J. Yuan, W. Deng, et al., "High-efficiency Organic Solar Cells With Low Non-Radiative Recombination Loss and Low Energetic Disorder," *Nature Photonics* 14 (2020): 300–305, https://doi.org/10.1038/s41566-019-0573-5.

149. Y. Xie, W. Wang, W. Huang, et al., "Assessing the Energy Offset at the Electron Donor/Acceptor Interface in Organic Solar Cells Through Radiative Efficiency Measurements," *Energy & Environmental Science* 12 (2019): 3556–3566, https://doi.org/10.1039/c9ee02939g.

150. Y. Xie, W. Liu, W. Deng, et al., "Bright Short-Wavelength Infrared Organic Light-Emitting Devices," *Nature Photonics* 16 (2022): 752–761, https://doi.org/10.1038/s41566-022-01069-w.

Supporting Information

Additional supporting information can be found online in the Supporting Information section.

Supporting File 1: adma73353-sup-0001-SuppMat.pdf.

Biographies

Nakul Jain is a postdoctoral fellow in Department of Physics, Chemistry and Biology (IFM) at Linköping University, Sweden. He received his master's degree in applied physics from the Malaviya National Institute of Technology Jaipur (India) in 2014 and his Ph.D. in physics from the Indian Institute of Technology Bombay (India) in 2020. His research focuses on the fundamental photo-physics of organic semiconductors, with particular emphasis on understanding charge-generation mechanisms and voltage losses in organic solar cells.

Xian'e Li is currently a postdoctoral researcher jointly affiliated with Lawrence Berkeley National Laboratory (with Dr. Slavomir Nemsak), the University of Oxford (with Prof. Iain McCulloch), and Linköping University (with Prof. Mats Fahlman). She received her B.S. in polymer materials and engineering (2015) and M.S. in materials science (2018) from Sichuan University, and her Ph.D. in applied physics (2023) from Linköping University. Her research focuses on surface and interface energetics in organic semiconductors, using UPS, XPS, AP-XPS, and NEXAFS to investigate charge generation, molecular packing, and energetic landscapes in organic solar cells and photocatalytic systems.

Mats Fahlman is a professor of Surface Physics and Chemistry in the Laboratory of Organic Electronics at Linköping University. He is active in the research of organic semiconductors using primarily surface science techniques to explore materials and interfaces as well as their effect on device properties.

Olle Inganäs is professor emeritus and Wallenberg scholar at Linköpings Universitet, Sweden. He received the Ph.D. in applied physics at Linköping University in 1984. He was an elected member of the Royal Swedish Academy of Sciences, class of physics, in 2006, a member of the Nobel committee for the prize in physics in 20122016, and chairman in 2016.

Koen Vandewal obtained his Ph.D. in Physics at Hasselt University in 2009 studying the device physics of organic photovoltaics. After that, he has been working for two years as a Postdoctoral Fellow at Linkoping University in Sweden and another two years at Stanford University in the US. In 2014, he was appointed as endowed professor at the Technische Universitaet (TU) Dresden in Germany. In January 2018, he moved from TU Dresden to Hasselt University in Belgium, leading a research group with the aim to solve fundamental questions in the field of organic, hybrid and molecular electronics with relevance to applications in opto-electronic devices, including solar cells and sensors.

Feng Gao is a professor and Wallenberg scholar at Linköping University in Sweden. He received his Ph.D. from the University of Cambridge (UK) in 2011, followed by a Marie Curie postdoc fellowship at Linköping University. His group currently focuses on the research into solution-processed energy materials and devices, mainly based on organic semiconductors and metal halide perovskites.